Version of Record: https://www.sciencedirect.com/science/article/pii/S0022169420300706
Manuscript_7f358828df6cfc191b08861e4577ced6

Elevation and spatial structure explain most surface-water isotopic variation across five Pacific Coast basins

L.M. McGill[1*], E.A. Steel[2], J.R. Brooks[3], R.T Edwards[4], A.H. Fullerton[5]

[1]Quantitative Ecology and Resource Management, University of Washington, Seattle, WA 98105, USA

[2]Pacific Northwest Research Station, USDA Forest Service, 400 NW 34th Street, Suite 201, Seattle, WA 98103, USA.

[3]Western Ecology Division, National Health and Environmental Effects Research Laboratory, U.S. Environmental Protection Agency, 200 SW 35th Street, Corvallis, Oregon 97333, USA

[4]Pacific Northwest Research Station, USDA Forest Service, 11175 Auke Lake Way, Juneau, AK 99801, USA

[5]Fish Ecology Division, Northwest Fisheries Science Center, National Marine Fisheries Service, NOAA, 2725 Montlake Blvd E, Seattle, WA 98112, USA

[*]Corresponding author: lmcgill@uw.edu

© 2020 published by Elsevier. This manuscript is made available under the Elsevier user license
https://www.elsevier.com/open-access/userlicense/1.0/

1 Introduction

Isoscapes are a framework that describe the spatial patterns in isotopic ratios across a landscape and are useful for addressing a variety of basic and applied research questions (West et al. 2010; Bowen and Good 2015). Stable isotopes of oxygen and hydrogen can be harnessed to determine source-water contributions to streamflow on a range of spatial and temporal scales (Rock and Mayer 2007; Koeniger et al. 2009; Wang et al. 2009; Mountain et al. 2015), estimate mean transit times (McGuire et al. 2005; McGuire and McDonnell 2006; Jasechko et al. 2016), delineate animal migration paths (Chamberlain et al. 1997; Hobson and Wassenaar 1997), and understand hydrologic flow paths (Rodgers et al. 2005; Singh et al. 2016; Nikolas et al. 2017). Despite the widespread use of water isotope ratios in research and their potential application for predicting future flows under a changing climate or identifying likely areas of cool water for fisheries management, few studies have compared drivers of variation in isotopic ratios at the basin scale or across basins.

The generation of accurate isoscapes is possible in part because water stable isotope ratios exhibit systematic spatial and temporal variation resulting from the process of isotope fractionation that accompanies water cycle phase changes and diffusion. Isotope fractionation is the primary force acting to produce variations in $\delta^{18}O$ and $\delta^{2}H$ values (both spatially and temporally) in water sources across the globe (Gat 1996; Araguas-Araguas et al. 2000). An example of this process is the Rayleigh rainout effect, wherein progressive isotopic depletion of a vapor cloud occurs as it moves along its storm trajectory. Rayleigh rainout occurs because heavy isotopes preferentially fall as precipitation (Dansgaard 1964; Clark and Fritz 1997). As a result, both precipitation and surface water isotopic ratios of $\delta^{18}O$ and $\delta^{2}H$ are highly correlated with changes in elevation, latitude, and longitude (Yonge et al. 1989; Ingrahm and Taylor 1991;

47 Dutton et al. 2005; Lechler and Niemi 2011), although the strength and presence of these
48 relationships can vary among river basins due to local processes such as evaporation (Bowen and
49 Good 2015).

50 Although broad-scale patterns in water isotopic ratios are well documented, when
51 generating isoscapes for use in water resource management, basin-scale factors that may affect
52 isotope distributions must be incorporated. Previous studies have shown consistent relationships
53 between elevation and surface water stable isotopes at the basin scale (Biggs et al. 2015; Peng et
54 al. 2015; Vespasiano et al. 2015; Fan et al. 2016). When the elevation-isotope relationship is
55 clear and consistent, water isoscapes can be a valuable tool for assessing the proportion of water
56 that comes from high elevation, climate sensitive snowmelt that is often critical for sustaining
57 summer baseflow in mountainous regions (Barnett et al. 2005; Brooks et al. 2012). However,
58 within certain regions, the elevation-isotope relationship is weak, absent, or inverse (Wassenaar
59 et al. 2009; Lechler and Niemi 2011; Bershaw et al. 2012), suggesting that local atmospheric or
60 hydrologic mechanisms are overriding the elevation effect within these regions. Basins in close
61 geographic proximity can have fundamentally different relationships between surface water
62 isotope ratios and elevation (Brooks et al. 2012; Nikolas et al. 2017). Therefore, cross-basin
63 analyses are needed to describe the variation in the landscape covariates that are highly
64 correlated with surface water isotope ratios in order to identify where and how isotopic variation
65 can be leveraged to identify distinct water sources within a river basin.

66 Previous studies have predominately generated water isoscapes in two-dimensional
67 space. Such models may be appropriate for terrestrial, oceanic, or atmospheric systems such as
68 precipitation over the continental United States or the surface of the Atlantic Ocean (Vachon et
69 al. 2010; McMahon et al. 2013). The movement of stream surface water, however, is constrained

by the topology of the dendritic stream network, which strongly affects the distribution of surface water stable isotopes that are conserved as water moves downstream (Clark and Fritz 1997). To date, isoscapes of stream networks have largely relied on interpolation using Euclidean distance (the straight-line distance between two sites) and have been restricted to predicting inputs from the local catchment (Brooks et al. 2012; Katsuyama et al. 2015). Although Bowen et al. (2011) modeled continuous river water isotope values by accumulating elevation-explicit, gridded precipitation isotope maps downstream and correcting them with model residuals, no explicit statistical method was used to partition the effects of downstream transport versus landscape predictors such as geology. Given that typical models do not account for the branching structure of stream networks, longitudinal connectivity, or flow direction, they may be inappropriate for use on river networks.

Ver Hoef et al. (2010) developed a class of geostatistical models, spatial stream network models (SSNMs), which account for spatial dependencies across stream networks. SSNMs are similar to conventional linear mixed models in that the deterministic mean of the dependent variable is modeled as a linear function of explanatory variables. However, the assumption of independent errors is relaxed and an atuocovariance model is used to account for spatial autocorrelation in the errors (Ver Hoeft et al. 2006; Peterson and Ver Hoef 2010; Ver Hoef and Peterson 2010). The autocovariance model can be specified using any combination of tail-up, tail-down, or Euclidean autocovariance functions. Tail-up and tail-down functions use hydrologic rather than Euclidean distance, and, in the tail-up model, spatial autocorrelation is restricted to flow-connected locations (i.e., water flows from an upstream location to a downstream location). SSNMs have been applied to answer a broad suite of questions, in each case improving model fit by explicitly modeling spatial autocorrelation in the data (Isaak et al.

93 2014; Brennan et al. 2016; Filipe et al. 2017). Application of these models to water isotopes
94 might provide information on the relative influence of environmental versus spatial processes on
95 isotope distribution, improve estimation of the covariates-isotope relationship absent
96 confounding spatial autocorrelation, and generate more robust predictions of isotope values at
97 unmeasured sites.
98 In this study, we compare the spatial patterns of surface water isotopes across five basins
99 within Washington and Southeastern Alaska to quantify and compare local controls on isotopic
100 variability of surface water and to explore the utility of applying simple elevation regressions
101 models for estimating water source across river basins. We also compare the performance of
102 models with and without network-based spatial autocorrelation. Specifically, the objectives of
103 our study are (1) to compare the strength with which isotope ratios vary by mean watershed
104 elevation (MWE) across five river basins, (2) to assess and compare whether additional
105 landscape predictors improve models of isotope ratios across basins, and (3) to explore where
106 SNNMs might be used to improve river water isoscape generation.
107
108 **2 Methods**
109 2.1 Study sites
110 We selected five climatically and geographically distinct watersheds across Washington and
111 Alaska (Figure 1). The Washington river basins (Snoqualmie, Skagit, Green, and Wenatchee) are
112 within the Cascade Range with the Wenatchee River draining to the east (leeward), and the other
113 three rivers draining to the west (windward). Western Washington has a Mediterranean climate
114 with dry summers and wet, mild winters influenced by its proximity to the Pacific Ocean.
115 Eastern Washington has a Continental climate with warmer summers, colder winters, and

116 comparatively less precipitation (Mote and Salathé 2010). The Alaska river basin, Cowee Creek,
117 has a Temperate Rain Forest climate characteristic of higher latitudes with cold, wet winters and
118 cool, wet summers. Precipitation in all regions occurs predominately from October to March and
119 falls as snow or rain, depending on latitude, elevation, and proximity to the Pacific Ocean.
120 Precipitation within all basins originates from vapor coming from the Pacific Ocean. Average
121 climate and physical characteristics for each basin are displayed in Table 1.

122 The Snoqualmie River begins as three distinct forks in the Mt. Baker-Snoqualmie National
123 Forest and drains 1,793 km^2 on the west side of the Cascade Range, Washington. The three forks
124 originate in forested public land before converging and flowing through a mix of agricultural,
125 residential, and commercial land use. On one major tributary, the Tolt River, a dam and a large
126 reservoir exist that provide drinking water for the City of Seattle.

127 The Green River drains a 1,185 km^2 watershed on the west side of the Cascade Range,
128 Washington. During the 19^{th} and 20^{th} centuries there was extensive railroad and logging activity
129 in the upper Green River valley; however, it has now become a gated water supply for the city of
130 Tacoma via damming of the river at the Howard Hansen Dam. The lower portion of the river
131 flows through downtown Seattle and is heavily modified and urbanized.

132 The Skagit River drains 8,163 km^2 of the western Cascade Range before emptying into Puget
133 Sound. It originates from headwaters in southwestern British Columbia and flows southwest
134 before meeting up with the Sauk River, which flows northwest and drains the North Cascades.
135 Five major hydropower projects are present on the Upper Skagit its tributaries. The river
136 experiences year-round glacial influence from numerous mountains, including Mount Baker and
137 Glacier Peak, both of which exceed 3,200 m.

The Wenatchee River drains 3,440 km^2 of the eastern Cascades before flowing into the Columbia River. Land use is similar to that of other basins, wherein the headwaters originate in forested public lands before flowing through a mix of agricultural, residential, and commercial land use. As described above, the climate on the east side of the Cascades is drier than that of the west side; however, the prevailing westerly winds, which cross the Cascades, create temperature and precipitation patterns that vary widely across the Wenatchee basin. For example, annual precipitation on the crest of the mountains averages over 2,900 mm, the majority of which falls as snow, while eastward and at only 780 meters, the city of Wenatchee averages less than 235 mm of annual precipitation.

Cowee Creek drains 118 km^2 of the United States Forest Service Héen Latinee Experimental Forest located in the Tongass National Forest, Alaska. The watershed is approximately 15% glaciated and experiences substantial influence from three alpine glaciers (18.2-km^2) and extensive perennial snowfields. The glaciers are rapidly diminishing and loss of the cool summer discharge from glacial melt is a concern in fish habitat management. Cowee Creek is characteristic of the thousands of moderately sized watersheds that drain the Coast Mountains of Alaska and British Columbia, and encompasses perennial snowfields, alpine meadows, spruce-hemlock forests, and extensive valley-bottom wetlands.

2.2 Data collection and processing

We collected between 31-58 spatially distributed water samples within each of our five basins in Summer 2017 during baseflow (Figure 1). Sampling sites within each basin were selected to include a mix of mainstem and tributary locations and to span the geographic and elevation range found within each basin. Water samples were collected within wading distance

161 from the stream edge, but in flowing current. Samples were collected in 20 ml vials with conical
162 plastic cap inserts to prevent evaporation, and duplicates were collected for every 20th sample.
163 Watersheds for each sampling point were delineated and landscape variables describing
164 the watersheds were derived from commonly available geostatistical products (Table 2). We
165 chose candidate covariates that were known to influence water isotope fractionation in some
166 basins, e.g., elevation and longitude (Dansgaard 1964; Clark and Fritz 1997), as well as those
167 that had some mechanistic basis for influencing isotopic ratios, e.g., aquifer and soil permeability
168 (Tauge and Grant 2009; Nickolas et al. 2017). Covariates examined include catchment area,
169 (MWE), latitude, longitude, mean annual precipitation (MAP), mean annual air temperature
170 (MAT), aquifer permeability, and soil permeability (Table 2).
171 Water isotopes were analyzed on a Laser Absorption Water-Vapor Isotope Spectrometer
172 (Model 908-0004, Los Gatos Research, Mountain View, CA) located at the Integrated Stable
173 Isotope Research Facility at the Western Ecology Division of the Environmental Protection
174 Agency, Corvallis Oregon. Oxygen and Hydrogen isotope ratios are reported as delta (δ) values
175 and presented in parts per thousand (‰) deviation from the adopted standard representing mean
176 isotopic composition of the global ocean (Vienna Standard Mean Ocean Water). Measurement
177 precision estimates (±1 standard deviation) were determined on repeated measures of both field
178 and lab duplicates and was 0.12‰ for $\delta^{18}O$ and 0.17‰ for $\delta^{2}H$. Deuterium excess (d-excess =
179 $\delta^{2}H - 8\delta^{18}O$; Dansgaard 1964) is a measure of the evaporative influence on water isotopes. The
180 global meteoric water line (GMWL) has a d-excess value of 10‰, but precipitation events vary
181 around this value. Based on d-excess variance in a 14-year record of precipitation isotopes
182 collected in Corvallis OR, we considered samples with d-excess values below 5‰ to have been

183 influenced by evaporation since falling as precipitation and removed those values from our
184 analyses.
185
186 2.3 Data analysis
187 In all five basins, we first conducted exploratory and mapping analyses to understand and
188 display the spatial distribution of landscape covariates (Table 2). We examined maps of and
189 correlations between landscape covariates to understand the distribution of and relationships
190 between predictor variables within and across watersheds. The goal of these exploratory analyses
191 was to understand underlying collinearity between covariates that might hinder our ability to
192 interpret statistical models.
193 We then examined relationships between landscape covariates and isotope values using
194 exploratory single variable analyses and explanatory multiple regression models. As $\delta^{18}O$ and
195 $\delta^{2}H$ values are highly correlated (Clark and Fritz 1997), all regression analyses considered only
196 $\delta^{18}O$ values. We used ordinary least squares regression to fit a linear model to each basin
197 independently; the model explained variation in isotope ratios as a function of a single landscape
198 characteristic (for the exploratory analyses) or suites of landscape characteristics (for the
199 explanatory models). For each univariate model, we conducted a t-test to test whether or not the
200 regression coefficient was statistically different from zero. An alpha level of 0.001 was chosen to
201 indicate a significant relationship. A conservative cutoff was chosen because of the large
202 quantity of statistical tests necessary to explore all potential predictors.
203 To identify the suite of landscape characteristics most closely associated with $\delta^{18}O$
204 values, we constructed a best fit multiple regression model for each basin. We selected variables
205 in our final best-fit models using a modified forward stepwise regression where we always

206 included MWE, if significant in the univariate model, as the first term in the models. Only
207 predictors significant at the univariate level were additionally considered for inclusion. We did
208 not include landscape predictors highly correlated with predictors already in the model (pairwise
209 correlation > 0.8). To constrain the number of statistical tests, total size of each model was
210 limited to four covariates and only main effects were examined. Covariates were individually
211 added to the model if they reduced the RMSE more than other potential covariates, were
212 significant at the univariate level, and increased the overall coefficient of determination (R^2). For
213 each best-fit model, we calculated the R^2 and the root mean squared prediction error (RMSPE)
214 using leave one out cross validation (LOOCV). To quantify variable importance in models with
215 more than one covariate, we calculated the independent effect of each covariate by comparing
216 the fit of all models containing a particular covariate to the fit of all nested models lacking that
217 covariate, through the process of hierarchical partitioning (Murray and Conner 2009; Walsh and
218 MacNally 2013). The resulting independent effect weights represent the average contribution of
219 each covariate to the variance in $\delta^{18}O$ values over all possible models, and are an estimate of the
220 proportion of variance in $\delta^{18}O$ values explained by each covariate.
221 In the Snoqualmie and Wenatchee basins, we further modeled the spatial relationship of
222 $\delta^{18}O$ values using semivariograms and SSNMs. We chose to test the use of spatial tools in the
223 Snoqualmie and Wenatchee as these basins are similar in size and network configuration, but
224 differ in the amount of isotopic variation explained by covariates. Semivariograms depict how
225 the semivariance, or average variation between measurement values separated by some distance,
226 changes in relation to the distance separating them. Semivariograms are useful for visualizing
227 patterns of spatial autocorrelation in the measured data and model residuals. Low semivariance
228 values indicate that sample pairs within some distance are similar, whereas high values indicate

dissimilar sample pairs. If positive autocorrelation occurs within a data set, the semivariance values are smallest at short distance lags and increase with distance. We displayed and compared two measures of distance between points: flow-connected distance (a network-based measure) and Euclidean distance (a straight-line measure). Semivariograms of the network-based distance consider only the topological distance between sites and illustrate how relationships between sites change when flow-connectedness is taken into account. Semivariograms of Euclidean distance reveal interactions or lateral connectivity between the stream network and the landscape. Semivariance was calculated using the robust estimator (Cressie 1993). We estimated the semivariogram at lag distances whose bins contained >10 site-pairs and that were less than half the maximum flow-connected distance between sites (Zimmerman and Ver Hoef 2016). We examined semivariograms to visualize dependencies in both raw $\delta^{18}O$ values and residuals from the best-fit linear models and SSNMs. Semivariograms were compared to one another to identify scales of spatial autocorrelation (McGuire et al. 2014; Brennan et al. 2016).

The SSNMs described in Ver Hoef and Peterson (2010) extend the standard linear model as:

$$Y = X\beta + z_{TD} + z_{TU,} + z_{EUC} + \varepsilon$$

where Y is a vector of the response (i.e. isotope ratios), X is a matrix of predictors (i.e. covariates from Table 2), β is a vector of estimated coefficients, z_{TD}, $z_{TU,}$ and z_{EUC} are the tail-down, tail-up, and Euclidean autocovariance models, and ε is a vector of independent normally distributed random errors. We followed a two-step procedure in fitting the SSNMs (Peterson and Ver Hoef 2010). First, we selected fixed effects while maintaining a constant spatial component consisting of exponential tail-up and exponential Euclidean spatial autocovariance functions. Fixed effects in our final SSNMs were selected independently of the linear model approach, but were selected

according to the same process described above for best-fit linear models. Second, we used Akaike Information Criterion (AIC) to select a covariance structure while maintaining the fixed effect(s) selected in the first step. We considered models having four possible spatial components: an exponential tail-up and Euclidean covariance structure, an exponential covariance structure alone, an exponential tail-up covariance structure alone, and a nugget-only model (i.e. assuming no spatial autocorrelation). We examined the predictive accuracy using LOOCV, and calculated the R^2, AIC, and RMSPE. We also decomposed the variation explained in each model into the proportion explained by the predictors and by the covariance structure in order to examine how each component contributed to model fit. Although the SSNM framework can include a mixture of autocovariance models based on tail-up, tail-down (i.e., based on network distance of flow-unconnected sites), and Euclidean distance, we chose to consider only tail-up and Euclidean (Steel et al. 2016; Steel et al. 2018). We elected to do this as isotopes move in a downstream direction and we had no reason to believe that any explanatory power achieved by using a tail-down covariance structure would reflect the underlying mechanism. All data analyses were conducted in R (http://cran.r-project.org) using the Spatial Stream Network (SSN) package (Ver Hoef et al. 2014) and Spatial Tools for the Analysis of River Systems (STARS) toolbox in ArcGIS 10.6 (Peterson and Ver Hoef 2014).

3 Results

3.1 General description and relationships with MWE

The measured $\delta^{18}O$ and $\delta^{2}H$ values in stream water samples ranged from -16.50 ‰ to -9.37 ‰ (mean = -12.85 ‰) and from -119.93 ‰ to -66.33 ‰ (mean = -92.42 ‰) respectively. In general, the highest values were found in the Snoqualmie and Green Rivers and the lowest values

275 in the Wenatchee River. Only three samples in our analysis had d-excess values less than 5 ‰.
276 All of these samples were collected in the Snoqualmie basin from streams that drained small,
277 stagnant ponds and were removed from further analyses. After their removal, the measured d-
278 excess values in stream water samples ranged from 5.01 ‰ to 15.43 ‰ (mean = 10.28 ‰).
279 The regression models between MWE and isotopic signature displayed an inverse
280 relationship for all basins except the Wenatchee River, which displayed no relationship (Figure
281 2). The δ^{18}O-MWE slopes for the regression models using both mainstem and tributary sites
282 were -2.5 ± 0.13 ‰ km^{-1} (R^2 =0.90) for the Snoqualmie River, -2.2 ± 0.20 ‰ km^{-1} (R^2 =0.82) for
283 the Green River, -4.4 ± 0.66 ‰ km^{-1} (R^2 =0.49) for the Skagit River, and -1.7 ± 0.28 ‰ km^{-1} (R^2
284 =0.48) for Cowee Creek. For the Wenatchee River, the R^2 value was 0.05 and the δ^{18}O-MWE
285 slope was -0.4 ± 0.41 ‰ km^{-1}. In four basins, tributaries and mainstem samples fall together on
286 the same regression, but in the Skagit River, mainstem samples have lower isotopic values for a
287 given MWE than smaller tributaries.
288
289 3.2 Landscape covariates
290 The structure of landscape covariates differed dramatically across basins and impacted
291 our ability to model δ^{18}O values as a function of landscape covariates (Figure 3). In the
292 Snoqualmie and the Green basins, most landscape predictors were highly correlated with one
293 another. For example, in the Snoqualmie basin, MWE had a correlation coefficient greater than
294 or equal to 0.75 with all landscape predictors except area and latitude. Similarly, in the Green
295 basin MWE had a correlation coefficient greater or equal to 0.69 with all landscape predictors
296 except area. In the Skagit, Wenatchee and Cowee basins, correlation among landscape
297 predictors existed, but was less extreme. In the Skagit basin, no correlation among predictors

298 exceeded 0.75, with the exception of MAT and MWE, which were almost perfectly correlated (-
299 0.98). Additionally, the Skagit is the only basin in which MAP and MWE were negatively
300 correlated (Figure 3). The Wenatchee basin displayed the lowest average correlation among
301 landscape predictors. Only longitude was moderately correlated (greater than 0.40) with all
302 landscape covariates except soil and aquifer permeability. In Cowee basin, there was a tight
303 coupling among MWE, MAP, and MAT where all correlations exceeded 0.92; however, beyond
304 these relationships no correlation exceeded 0.55.
305
306 3.3 Univariate and best-fit linear models
307 The direction and magnitude of relationships between $\delta^{18}O$ and $\delta^{2}H$ values and landscape
308 covariates varied across basins (Figure 3). For example, in the Snoqualmie and Green basins,
309 $\delta^{18}O$ and $\delta^{2}H$ values were highly negatively correlated with mean annual precipitation (MAP) (-
310 0.85, -0.69 for $\delta^{18}O$ and -0.80, -0.72 for $\delta^{2}H$), while in the Skagit, Wenatchee and Cowee basins
311 this relationship was reversed (0.86, 0.44, 0.76 for $\delta^{18}O$ and 0.87, 0.67, 0.66 for $\delta^{2}H$). We note
312 again that the high collinearly of landscape predictors within basins made it difficult to parse
313 apart some effects.
314 Best-fit models for all basins included MWE but displayed clear differences in both level
315 of complexity and predictive accuracy. In the Snoqualmie, Green and Cowee basins, best-fit
316 models included only MWE (Table 3). Calculated R^2 values were 0.90 for the Snoqualmie, 0.82
317 for the Green, and 0.48 for Cowee. The RMSPE for these models was 0.26, 0.36 and 0.42 ‰,
318 respectively. In the Skagit and Wenatchee basins, on the other hand, incorporating additional
319 predictors beyond MWE increased the amount of variance explained in our isotope data.
320 Additional covariates included in the Skagit model were MAP, area, and aquifer permeability,

while the only additional covariate included in the Wenatchee model was longitude (Table 3). The Skagit River, similar to other west side basins, displayed high predicative accuracy (R^2 =0.87; RMSPE=0.41 ‰) whereas the Wenatchee River displayed low predictive accuracy (R^2=0.47; RMSPE=0.42 ‰). Independent effect weights for the Skagit model shows a relatively even partitioning of variance among all predictors (I_{elev} = 21 %, I_{precip} = 33 %, I_{area}= 26 %, I_{perm}= 20 %), whereas in the Wenatchee model the majority of variation in $\delta^{18}O$ values is explained by longitude (I_{lon} = 70 %, I_{elev}= 30 %).

3.4 Semivariograms and spatial stream network models

The Snoqualmie and Wenatchee basins showed spatial dependencies for raw $\delta^{18}O$ values (Figure 4). For the Snoqualmie basin raw $\delta^{18}O$ values, semivariance for Euclidean distance (i.e. the straight line distance between all sites) increased rapidly and linearly before leveling off around 35 km. This change in semivariance suggests that sites beyond 35 km apart were uncorrelated, while sites closer together were more highly correlated with one another. Semivariance for flow-connected sites (i.e. the network distance between sites that share flow) for raw $\delta^{18}O$ values was generally much smaller and increased slowly with distance. Furthermore, semivariance of raw $\delta^{18}O$ values between flow-connected sites never leveled off, suggesting the presence of an unmodeled trend such as MWE. Similar patterns of semivariance were apparent in the Wenatchee basin raw $\delta^{18}O$ values, although overall values and the difference between the magnitude of Euclidean and flow-connected semivariance were both smaller. In addition, the semivariance for the Euclidean distance leveled off at around 25 km in the Wenatchee basin.

343 We compared model fit and variance decomposition for SSNMs with four distinct
344 autocovariance models (Table 4; Figure 5; Figure 6). For the Snoqualmie basin, similar to the
345 best-fit linear model, only MWE was selected as a fixed effect, capturing between 81-90 % of
346 the variance in $\delta^{18}O$ values (Table 4; Figure 6). When spatial autocorrelation was explicitly
347 accounted for by including a covariance structure in the model, the total variance explained was
348 greater than the non-spatial model; however, between 3-9 % of the variance previously explained
349 by the covariates was shifted onto the covariance structure (Table 4; Figure 6). The SSNM with
350 a tail-up covariance structure outperformed all others and had the lowest AIC, RMSPE and R^2.
351 RMSPE decreased from 0.26 ‰ in the linear model to 0.16 ‰, similar to analytical precision
352 (0.12 ‰), and R^2 increased from 0.90 in the linear model to 0.96 (Table 4). Adding a Euclidean
353 covariance structure did not improve prediction accuracy as much as the tail-up model.
354 For the Wenatchee basin, longitude and MWE were again selected as fixed effects,
355 explaining 45-47 % of the variation in $\delta^{18}O$ values, significantly less variation than in the
356 Snoqualmie models. Spatial autocorrelation explained an additional 14-26 % of the variance not
357 explained by covariates. Contrary to the Snoqualmie basin, models that included a Euclidean
358 covariance structure outperformed all others and had the lowest AIC, RMSPE, and R^2,
359 suggesting that network structure was less important in this basin (Table 4; Figure 6). Including
360 both tail-up and Euclidean covariance structures improved the R^2 and RMSPE over the simple
361 Euclidean model (0.71 vs 0.67 and 0.31 ‰ vs 0.33 ‰, respectively), but resulted in a nearly
362 identical AIC value (51.67 vs. 51.24, respectively). Although the models are comparable, we
363 selected the model with both a tail-up and Euclidean covariance structure to move forward with
364 further analyses.

Semivariograms of spatial and linear model residuals displayed a reduction in semivariance as compared to the raw data for both basins and distance measures (Figure 4). This reduction suggests that by accounting for spatially structured covariates such as MWE and longitude, regression models remove some spatial autocorrelation. The decrease in semivariance between raw data and linear residuals was more pronounced for the Snoqualmie basin, whereas the decrease in semivariance between linear and spatial residuals was more pronounced for the Wenatchee basin. For both the Snoqualmie and Wenatchee basins, semivariance of spatial model residuals is relatively flat. This pattern suggests that accounting for spatial structure through SSNMs removes the majority of spatial autocorrelation in the $\delta^{18}O$ values.

4 Discussion

4.1 MWE gradient

Although we expected MWE to be the main determinant of isotopic variation in surface water, our analysis revealed differences in surface water MWE-$\delta^{18}O$ slopes between basins based on basin size, shape and location on the windward and leeward sides of mountains. The strong elevation gradient observed in western Washington basins and Cowee Creek, all of which drain windward mountainsides, can be attributed to the rainout effect, or Rayleigh distillation (Dansgaard 1964; Clark and Fritz 1997). Storms bringing precipitation to western Washington and coastal Alaskan basins originate from the Pacific Ocean and move eastward. Continued rainout produces isotopically depleted precipitation at higher elevations, with the most depleted precipitation found at the crest. Close proximity to the Pacific Ocean exacerbates the rainout process. As the warm, wet air mass travels up the Cascade and Alaskan Coast Mountains, it experiences orographic lifting and adiabatic cooling, resulting in increased precipitation and the

388 observed elevation trends. Similar to most other studies globally, our observed δ^{18}O-MWE
389 relationship is close to linear over the sampled elevation range for windward basins (Poage and
390 Chamberlain 2001). The combination of processes dominantly responsible for isotopic
391 distillation during rainout behaves linearly over much of the world; however, basin specific
392 processes such as mixing of baseflow sources from differential geologies may contribute to
393 differences in δ^{18}O-MWE slopes and proportion of isotopic variation explained by MWE across
394 basins.

395 Several studies have found global average isotopic-elevation relationships, or lapse rates,
396 for precipitation, snow, and river water between -2.1 ‰ km^{-1} and 2.9 ‰ km^{-1}, except at latitudes
397 greater than 70° where isotopic lapse rates are higher (Poage and Chamberlain 2001; Bowen and
398 Wilkinson 2002; Dutton et al. 2005). In our study the Snoqualmie and Green basin δ^{18}O-MWE
399 slopes fall within this range (-2.5 ± 0.13 ‰ km^{-1} and -2.2 ± 0.20 ‰ km^{-1}, respectively). The
400 similar δ^{18}O-MWE slopes of the Green and Snoqualmie Rivers are likely due to the close
401 geographic proximity of the basins and similar orientation with respect to incoming coastal
402 weather. Additionally, MWE explains most of the variation in isotope ratios for the Snoqualmie
403 and Green Rivers, indicating that elevation-induced rainout is the greatest control on δ^{18}O
404 values. The higher δ^{18}O-MWE slope of the Skagit River is surprising, given its close proximity
405 to the Green and Snoqualmie basins, but this basin has unique attributes discussed in the next
406 section. Our observed δ^{18}O-MWE slope for Cowee Creek was lower (-1.7 ± 0.28 ‰ km^{-1}) than
407 windward Washington basins even though MWE was the only significant driver. However,
408 Cowee basin is small and glaciated and samples were collected over several months. This is
409 further discussed in the next section. Even though MWE was a strong driver of isotopic variance,
410 each windward basin responded uniquely, reiterating the importance of basin specific isoscapes.

411 We did not observe a large $\delta^{18}O$-MWE slope in the Wenatchee basin, which is located on
412 the leeward side of the Cascade Range. For leeward basins, if precipitation results from
413 continued rainout of air masses as they traverse topographic barriers, then continued Rayleigh
414 distillation on the leeward slope should produce an inverse relationship with altitude. Although
415 less prevalent in the literature than windward, orographically induced rainout (Poage and
416 Chamberlain 2001), inverse or ambiguous $\delta^{18}O$-elevation relationships have been reported from
417 leeward slopes in the Sierra Nevadas (Friedman and Smith 1970) and the Canadian Rockies
418 (Grasby and Lepitski 2002; Moran et al. 2007) for precipitation isotopes, and from the Oregon
419 Coast Range for stream water isotopes (Brooks et al. 2012; Nikolas et al. 2017). Potential
420 reasons for the ambiguous $\delta^{18}O$-MWE relationship in the Wenatchee basin are threefold. First,
421 the amount of precipitation falling in the Wenatchee basin is lower than in west side basins (e.g.
422 Snoqualmie MAP is 2,435 mm/year and Wenatchee MAP is 1,210 mm/year). Within this drier
423 climate, local evaporation of surface water could add to the atmospheric vapor or subcloud
424 evaporation could be influential, which would negate isotope depletion from the rainout effect.
425 Previous studies have documented this dampened rainout effect (Ingraham and Taylor 1991;
426 Guan et al. 2009; Wassenaar et al. 2009; Bershaw et al. 2012). However, we did not see the
427 changes in d-excess expected if subcloud evaporation were significant in the Wenatchee basin.
428 Second, although the Wenatchee samples show no systematic relationship with MWE alone,
429 when longitude, which is a proxy for distance inland, and MWE are included together in the
430 best-fit model, a $\delta^{18}O$-MWE slope similar to windward basins emerges, although longitude was
431 still the most important variable within the model. The Wenatchee basin is oriented north to
432 south and shares a long border with the Cascade crest (Figure 1). Consequently, the heaviest
433 precipitation occurs near the crest. As a vapor cloud moves eastward along the typical storm

434 trajectory, precipitation becomes more depleted as a result of rainout. Rainout with increasing
435 distance from the Pacific coast may counteract the less pronounced elevation gradient. Lastly,
436 turbulent atmospheric mixing of air masses as they are forced up and over the Cascade crest may
437 contribute to the lack of an observable δ^{18}O-MWE slope (Moran et al. 2007). More research is
438 needed into leeward basins to distinguish among these three potential factors.
439
440 4.2 Other drivers of observed isotope patterns
441 The Skagit basin was unique among the windward basins in that the best-fit model
442 included MAP, watershed area, and aquifer permeability as covariates in addition to MWE.
443 Orientation with respect to storm path alignment and topographic features of each basin likely
444 drive differences in the strength and slope of river ^{18}O-MWE slopes observed in windward
445 basins and resulted in the inclusion of MAP in the Skagit best-fit model (Scheihing et al. 2018).
446 The Green and Snoqualmie Rivers flow northwest. The Skagit River generally flows west;
447 however, the largest tributary to the Skagit, the Sauk, flows northwest (Figure 1; Figure S1). Due
448 to the rain-shadowing effects of Mt. Rainier and the Olympic mountains, southwestern Puget
449 Sound watersheds like the Green and Snoqualmie tend to receive maximum precipitation during
450 westerly air flow, while watersheds in the northwest Puget Sound like the Skagit tend to receive
451 maximum precipitation during west-southwesterly air flow (Neiman et al. 2011; Siler et al.
452 2013). As a result, precipitation and elevation gradients largely align in the Green and
453 Snoqualmie basins, with the greatest amount of precipitation occurring at high elevations leading
454 to strong covariation (Figure 3). In contrast, the greatest amount of precipitation in the Skagit
455 basin occurs at mid elevations on the western side of the basin, including in headwaters of the
456 Sauk and Baker Rivers (Figure S1). East of the mainstem Skagit dams, at some of the highest

457 elevations in the basin, precipitation amount declines substantially due to a rain shadow effect
458 produced by the high peaks of the Skagit Crest within the basin (Figure S1). Storms approaching
459 the Skagit basin on a west-southwesterly track reach the Sauk basin first as they move inland. As
460 they progress along their trajectory, continued rainout results in progressively more isotopically
461 depleted precipitation. The influence of complex precipitation patterns in the Skagit basin was
462 reflected in our data. Samples collected from the Sauk basin were systematically more
463 isotopically enriched than samples collected from the upper Skagit basin, even at identical
464 elevations. Additionally, in our best-fit model, MAP was positively related to $\delta^{18}O$ values,
465 indicating that in areas of high MAP isotope ratios were more enriched. High MAP at mid
466 elevations likely contributes to the high $\delta^{18}O$-MWE slope observed in the Skagit basin.
467 Basin attributes not examined within our modeling framework may influence isotope
468 ratios. Within the Skagit River, mainstem samples displayed the lowest isotope ratios, likely
469 indicating that the mainstem of the Skagit is fed by higher elevation source water than small
470 tributaries (Figure 2). The negative relationship between watershed area and $\delta^{18}O$ values in the
471 Skagit best-fit model reflects this, indicating that in large watersheds isotope ratios were more
472 depleted. Glaciation in the Skagit River points to the importance of high elevation glacial and
473 snowpack melt as a significant source of summer baseflow. Riedel and Larrabee (2016) found
474 that surface melt from glaciers contributes 6-12% of the Skagit River's total summer runoff, and
475 roughly twice that fraction in August and September. This same study also noted that glacial
476 meltwater is concentrated in the tributaries Thunder Creek, White Chuck River, Suiattle River,
477 Baker River, and Cascade River (Figure S1). Our Skagit River water samples showed $\delta^{18}O$
478 values below the average $\delta^{18}O$-MWE regression line for the outlets of the White Chuck and
479 Suiattle Rivers and isotope ratios above the average $\delta^{18}O$-MWE regression line for the Baker and

480 Cascade River outlets. We would expect samples to fall below the line if a greater proportion of
481 flow originated from high-elevation glacial meltwater. The presence of glacial meltwater and
482 snowmelt may have skewed the high elevation watersheds to lower isotopic ratios and may have
483 contributed to the high δ^{18}O-MWE slope observed in the Skagit basin.

484 Although the Cowee Creek basin is heavily glaciated, we did not observe the same
485 pattern of highly depleted mainstem isotope ratios present in the Skagit basin and watershed area
486 was not included in our best-fit model. This was surprising, as previous studies have found
487 seasonal patterns in δ^{18}O at the outflow of Cowee Creek that are consistent with an increase in
488 the proportion of streamflow derived from δ^{18}O-depleted snow and glacial melt in higher
489 elevation watersheds from late May into August (Fellman et al. 2014; Fellman et al. 2015).
490 Fellman et al. (2015) found an average δ^{18}O ratio of -14.5‰ at the outflow of Cowee Creek
491 across summer months (May – August) and δ^{18}O ratios below -15.0‰ through most of August,
492 reflecting the contribution of glacial meltwater (average δ^{18}O = -16.4‰), as the winter snowpack
493 is typically ablated by early summer. At the lowest site on Cowee Creek in our study, samples
494 collected in late May already had values (-15.5 ‰) that were as low as those measured in late
495 August during Fellman et al. (2015) study. The weak δ^{18}O-MWE relationship in Cowee Creek
496 could be because high elevation, glacial sources of water dominated the flow in most tributaries
497 sampled during our study. Higher resolution temporal sampling of the area is necessary to parse
498 these mechanisms.

499 Within the Snoqualmie and Green basins, all water isotopes samples fell upon a similar
500 MWE gradient, regardless if it was a small tributary, or mainstem samples that aggregate the
501 entire basin (Figure 2). The isotopic composition of river water samples is determined by water
502 isotopes in precipitation infiltrating into mountain blocks. The subsequent stream water is a

503 mixture of groundwater baseflows with different transit times. The tight δ^{18}O-MWE coupling
504 suggests summer baseflow derives from inputs more evenly dispersed throughout the basin,
505 potentially because of shallow groundwater influx (i.e., as opposed to deep groundwater
506 flowpaths or snowmelt sources). The isotopic composition of shallow groundwater does not
507 deviate significantly from the mean weighted annual composition of precipitation in temperate
508 climates in areas without seasonal or spatial bias in recharge (Clark and Fritz 1997; Bowen et al.
509 2011). In the Snoqualmie and Green basins, nearly all precipitation falls within the winter
510 months, and previous studies have not found significant seasonal differences in precipitation
511 isotopes ratios in the Pacific Northwestern USA (Brooks et al. 2012). Several studies find similar
512 patterns for summer baseflow (Yeh et al. 2014; Singh et al. 2016; Rautio et al. 2015). In contrast,
513 Brooks et al (2012) found that the mainstem Willamette River, and outlets of other large rivers
514 feeding the Willamette had isotopic values that were lower than the predicted elevation gradient
515 relationship estimated from small watersheds, which we also found in the Skagit River. They
516 interpreted this difference as a bias towards high elevation water sources dominating the flow
517 within the river, likely due to deep groundwater flowpaths within the Oregon High Cascades.
518 This suggests that the Green and Snoqualmie Rivers are much less dependent on high elevation
519 snowmelt for summer baseflow as compared to the Cascade rivers in Oregon, and the Skagit
520 River. Future studies should more explicitly consider the geologic context of each basin in order
521 to understand the interaction between potentially complex ground and surface water flowpaths.
522 Dams, reservoirs, and lakes are pervasive across our study basins and have the potential
523 to alter water storage and transport, thus impacting our interpretation of isotope values below
524 these structures. In our data, we found small differences when examining isotope ratios above
525 and below the Howard Hansen Reservoir and Lake Wenatchee. The Howard Hansen Reservoir

526 on the Green River and the Tolt Reservoir, a similar hydropower structure in the Snoqualmie
527 River, are operated for flood control in the winter, flow augmentation in the summer, and
528 provide drinking water year-round. The reservoirs fill in the late winter and spring, potentially
529 holding back winter precipitation and high elevation snowmelt and releasing it during summer
530 low flow. However, in our data isotope ratios of water sampled above the Howard Hansen
531 Reservoir ($\delta^{18}O$ = -11.92‰ and d-excess = 10.33) were only slightly more depleted than those
532 sampled at the outflow ($\delta^{18}O$ = -11.03‰ and d-excess = 7.24). Conversely, isotope ratios of
533 water sampled at the Lake Wenatchee outflow ($\delta^{18}O$ = -15.32‰ and d-excess = 11.29) were
534 more depleted than ratios from both the inflowing Little Wenatchee ($\delta^{18}O$ = -14.09‰ and d-
535 excess = 11.47) and White Rivers ($\delta^{18}O$ = -14.94‰ and d-excess = 10.16), which join together to
536 form Lake Wenatchee. The isotopic signature of the Lake Wenatchee likely reflects the long-
537 term average of river water input which may be more depleted than isotope ratios of September
538 river flows due to a large influx high-elevation snowmelt in Spring. Previous studies have found
539 muted temporal isotopic variation below artificial impoundments and natural lakes, reflecting
540 extended retention times and elevated river water mixing (Kendall and Coplen 2001; Wassenaar
541 et al. 2011; Brooks et al. 2012; Trinh et al. 2017). Although the retention time of water within
542 impoundments is an important consideration when interpreting downstream isotope ratios, our
543 results illustrate that despite the presence of extensive hydrologic modification within our basins,
544 isotopes can preserve signals of mainstem source water dynamics.
545
546 4.3 In-stream and landscape processes shape isotope values
547 Ours is one of the first studies to use a class of geostatistical models, Spatial Stream
548 Network Models (SSNM), to model stream water isotope ratios (but see Segura et al. 2019). The

549 SSNM approach also allowed us to model spatial correlation explicitly, taking advantage of the
550 unique topology of stream networks. Similar to studies of other ecological phenomena (Isaak et
551 al. 2014; Brennan et al. 2016; Filipe et al. 2017), water isotopic ratios on stream networks
552 showed substantial autocorrelation and predictive accuracy was improved by spatial models
553 compared to non-spatial models (Bowen et al. 2011; Table 4; Figure 5). Inherent covariation in
554 river basins can hinder statistical efforts to identify mechanistic links between landscape
555 gradients and features of aquatic ecosystems and result in negative consequences such as inflated
556 goodness-of-fit metrics and inflated error terms on key coefficients that may undermine model
557 building (Lucero et al. 2011). Linear regression assumes that each measurement is independent
558 from others and contains non-redundant information. Therefore, if measurements are spatially
559 autocorrelated, standard error estimates will be artificially small, tests of statistical significance
560 will be too liberal, and estimates of R^2 will be too large (Dale and Fortin 2009; Isaak et al. 2014).
561 SSNMs explicitly model spatial autocorrelation and therefore provide better estimates of the
562 effect of landscape covariates on isotope ratios.
563 For the Snoqualmie River, incorporating an autocovariance function accounting for the
564 branching river network structure resulted in modest improvements to model performance. Most
565 variation in $\delta^{18}O$ values was already explained by MWE, which is spatially-structured, resulting
566 in little residual variation or autocorrelation (Table 4; Figure 4). However, the best-fit model did
567 include a tail-up component, illustrating the importance of passive longitudinal transport of water
568 isotopes along stream networks. The dominance of MWE in the model likely occurs in part due
569 to the structure of landscape covariates in the Snoqualmie River. Most landscape predictors were
570 highly correlated with one another, and the influence on isotope ratios aligned in the same
571 direction (e.g. MWE and longitude were positively correlated). In basins such as the Snoqualmie,

572 where covariates covary strongly and the subsequent relationship between water isotopes and
573 covariates is simple, spatial models only slightly improve our understanding of river water
574 isoscapes.

575 In the Wenatchee River, on the other hand, incorporating spatial structure in Euclidean
576 space dramatically improved model performance. The role of covariates in the Wenatchee
577 models were limited, with fixed-effects explaining only 47% of variation in non-spatial models
578 and 45-49% of the variation in spatial models. Approximately two-thirds of the variance in the
579 best-fit SSNM could be attributed to fixed effects and one-third to spatial structure in the
580 Wenatchee model residuals (Table 4). The strong Euclidean component in the Wenatchee best-fit
581 model, illustrated by the large proportion of variation explained in Figure 6, suggests that linear
582 relationships with longitude and MWE were insufficient to describe landscape processes
583 influencing stream water isotope values (McGuire et al. 2014; Zimmerman and Ver Hoef 2017).
584 Landscape features affecting isotope ratios could include local geological features associated
585 with groundwater upwelling, beyond the general descriptor of aquifer permeability. Previous
586 studies have shown that geologic features, such as porous lava flows, sandstone, and earthflows,
587 and hillslope characteristics (e.g. slope and roughness) can influence baseflow isotopic
588 composition (Nicolas et al. 2017; Singh et al. 2016; Segura et al. 2019). Furthermore, in the
589 Wenatchee basin landscape covariates display little correlation with one another and often align
590 in opposing directions (e.g. MWE and longitude were negatively correlated). These competing
591 forces likely work against each other to create a complex isotopic landscape that is difficult to
592 model using standard linear models. In basins such as the Wenatchee, where the influence of
593 covariates on isotope signature is weak and covariates display little correlation with one another,

including spatial structure provided insight about the presence of key structuring processes that were unaccounted for in our covariate selection.

4.4 Study Limitations

As in any study, our ability to generalize results and make inferences about other watersheds is limited by our sampling design, dataset, and the models considered. In this study, water sample collection locations were limited to areas easily accessed by roads, and collection of samples across a large portion of the Upper Skagit basin into Canada did not occur. Increased spatial coverage would improve predictions of drivers of isotope ratios and allow us to consider a greater number of predictors in our analyses. Additionally, although we considered five basins across a single sampling season (summer low flow, 2017), only one basin was located on the leeward side of mountains.

Although our snapshot in time provides a picture of drivers of the isotope ratios during baseflow, it does not give insight into temporal variation in drivers of isotope signature. Several studies have found differences in drivers of isotope patterns across time (Liu et al. 2004; Payn et al. 2012), and therefore our results should not be generalized to other seasons. It should also be noted that while sampling of the Washington basins took place over no more than two weeks, Cowee Creek was sampled over the course of three months due to logistical challenges in accessing its remote sites by aircraft. Lastly, it is important to recognize that SSNMs are an extension of linear regression and both methods predict at unsampled locations using smoothed averages. Therefore, when we generated isoscapes, features not included in our sampling design (e.g. local point sources of groundwater) were not included.

4.5 Management Implications

Our study summarizes current knowledge of basin factors driving variability in surface-water isotope ratios and provides a foundation for future monitoring work as well as for leveraging the isotopic signature of surface water in river basins and fisheries management. We observed a strong MWE gradient across all rivers draining windward basins. Furthermore, in the Snoqualmie and Green basins MWE was highly correlated with other parameters known to drive isotopic ratios. In these basins, these simple MWE-based relationships permit easy interpretation of isotope data. Future work could harness the information they contain for river basin management, such as predicting the contribution of climate sensitive, high-elevation snowmelt to summer baseflow.

Changes to climate and hydrology are expected across the Pacific Northwest. Climate models predict substantial winter warming, leading to increased precipitation falling as rain and decreased snowpack, translating to increased winter river runoff and reduced summer baseflow discharge (Elsner et al. 2010). Measuring water stable isotopes would be a simple method for monitoring these changes over time.

Impacts of global change will be heterogeneous both within river basins and across the region, and understanding how high elevation water contributes to stream discharge across basins will be a valuable tool (Steel et al. 2018). For example, all basins in this study host populations of ESA-listed salmonids, which are limited by high summer temperatures and low flows. Resource managers could easily access and plot covariate data such as MWE, longitude, and MAP to determine in which basins these covariates are correlated, suggesting an easy to interpret isotope-MWE relationship. The same simple isotope-MWE relationship could also be applied to other midlatitude mountain ranges with prevailing westerly winds and a north-south

639 orientation, such as the Sierra Nevada, the southern Alps, and the southern Andes (Siler et al.
640 2013).

641 For Cowee Creek and the Skagit River, interpretation of water isotope monitoring within
642 the basins becomes more challenging. In the Cowee basin the $\delta^{18}O$-MWE slope was much lower
643 than expected. Temporal isotopic variance at the outlet may indicate the dominance of glacial
644 sources over time, and we sampled over a period of high glacial output. However, additional
645 sampling over a more condensed time period would be necessary for accurate interpretation. In
646 the Skagit Basin interpretation of isotopic variation is difficult, as the orographic rainout process
647 becomes complicated by the complex topography and sampling in the upper basin was limited.
648 In basins with similar accessibility issues, accurate isoscapes could help in monitoring the
649 proportion of streamflow derived from glacial and snowmelt and relieve some of the burden of
650 expensive field campaigns.

651 Our results provide guidance for future monitoring or research on stable isotopes in
652 surface waters. In the basins described above, with expected simple and strong relationships
653 between MWE and isotope values, fewer samples may be necessary to create customized and
654 effective models or management tools. In larger basins or in areas where complex local
655 atmospheric or hydrologic processes occur, greater temporal and spatial sampling may be
656 necessary in order to partition water sources in ways that are both isotopically distinct and
657 environmentally relevant.

658 Our study also provides guidance for understanding the types, advantages, and
659 disadvantages of methods for stream isoscape generation. We found that in basins where
660 correlation between covariates and isotope ratios is weak, spatial models can improve predictions
661 and demonstrate evidence of landscape level patterns not captured by non-spatial models. We

also found that in basins where covariates known to influence isotope signature correlate strongly with one another and are themselves highly spatially structured, spatial models do little to improve predictions. The choice to use spatial or non-spatial models should be determined by data availability and the relevant questions. Our results provide insight as to where the additional effort to build these models may be a particularly good investment.

5 Conclusions

In this study we demonstrated that elevation was the dominant predictor of isotope ratios across five Pacific Northwest basins, but the importance of elevation varied between basins and depended on geographic location, landscape attribute configuration, and basin size. Elevation explained a range of the isotopic variation in surface water across the five basins, but the nature of this relationship (δ^{18}O-MWE slope, other covariates) was different even between adjacent basins. Incorporating spatial structure though the SSNM framework captured aspects of water isotopic variation even in basins where variance explained by covariates was high. Spatial structure was particularly important to consider in the Wenatchee, our leeward side basin, where covariates explained the least of the isotopic variation. Our results illustrate that basin-specific models that include spatial structure improve accuracy of surface-water isoscapes for understanding hydrologic function, interpreting source contributions downstream, or assisting in basin management.

Acknowledgements

This research was funded by a Department of the Interior Northwest Climate Adaptation Science Center graduate fellowship awarded to Lillian McGill. This material is based upon work

685 supported by the National Science Foundation Graduate Research Fellowship under Grant No.
686 DGE-1762114. Any opinion, findings, and conclusions or recommendations expressed in this
687 material are those of the authors and do not necessarily reflect the views of the National Science
688 Foundation. This manuscript has been subjected to Agency review and has been approved for
689 publication. The views expressed in this paper are those of the author(s) and do not necessarily
690 reflect the views or policies of the U.S. Environmental Protection Agency. Mention of trade
691 names or commercial products does not constitute endorsement or recommendation for use. We
692 received helpful comments from Dr. Rose Smith and Dr. Jim Markwiese on earlier version of
693 this manuscript.
694

695 **References**

696 Araguás-Araguás L., Froehlich K., & Rozanski K. (2000). Deuterium and Oxygen-18 Isotope
697 Composition of Precipitation and Atmospheric Moisture*, Hydrological Processes,* 14(8):
698 1341–55.

699 Barnett, T.P., Adam, J.C., Lettenmaier, D.P. (2005). Potential impacts of warning climate on
700 water availability in snow-dominated regions, *Nature*, 438: 303-309.

701 Bershaw, J., Penny, S.M., & Garzione, C.N. (2012). Stable isotopes of modern water across the
702 Himalaya and eastern Tibetan Plateau: Implications for estimates of paleoelevation and
703 paleoclimate, *Journal of Geophysical Research,* 17: D02110.

704 Biggs T.W., Lai C.T., Chandan P., Lee R.M., Messina A., Lesher R.S., & Khatoon N. (2015).
705 Evaporative Fractions and Elevation Effects on Stable Isotopes of High Elevation Lakes
706 and Streams in Arid Western Himalaya*, Journal of Hydrology,* 522: 239–49.

707 Bowen G.J., & Good S.P. (2015). Incorporating Water Isoscapes in Hydrological and Water
708 Resource Investigations, *Wiley Interdisciplinary Reviews: Water,* 2(2): 107–19.

709 Bowen G.J., Kennedy C.D., Liu Z., & Stalker J. (2011). Water Balance Model for Mean Annual
710 Hydrogen and Oxygen Isotope Distributions in Surface Waters of the Contiguous United
711 States, *Journal of Geophysical Research,* 116: G04011.

712 Bowen G.J., & Wilkinson, B. (2002). Spatial distribution of δ18O in meteoric
713 precipitation, *Geology,* 30(4), 315-318.

714 Brennan, S.R., Torgersen, C.E., Hollenbeck, J.P., Fernandez, D.P., Jensen, C.K., & Schindler,
715 D.E. (2016). Dendritic Network Models: Improving Isoscapes and Quantifying Influence
716 of Landscape and in-Stream Processes on Strontium Isotopes in Rivers, *Geophysical*
717 *Research Letters,* 43(10): 5043–51.

718 Brooks, J.R., Wigington, P.J., Phillips, D.L., Comeleo, R., & Coulombe, R. (2012). Willamette
719 River Basin Surface Water Isoscape (δ18O and δ2H): Temporal Changes of Source
720 Water within the River, *Ecosphere,* 3(5): Article 39.
721 Chamberlain, C.P., Blum, J.D., Holmes, R.T., Feng, X., Sherry, T.W., & Graves, G.R. (1997).
722 The Use of Isotope Tracers for Identifying Populations of Migratory
723 Birds, *Oecologia,* 109(1): 132–41.
724 Clark, I.D., & Fritz, P. (1997). Environmental Isotopes in Hydrogeology. Boca Raton, FL: CRC
725 Press/Lewis Publishers.
726 Cressie, N. (1993). Statistics for spatial data. New York: John Wiley, 900 p.
727 Dale, M.R.T., & Fortin, M.J. (2009). Spatial autocorrelation and statistical tests: some solutions,
728 *Journal of Agricultural, Biological, and Environmental Statistics*, 14: 188-206.
729 Dansgaard, W. (1964). Stable Isotopes in Precipitation. *Tellus* 16(4): 436–68.
730 Dutton, A., Wilkinson, B.H., Welker, J.M., Bowen, G.J., & Lohmann, K.C. (2005). Spatial
731 Distribution and Seasonal Variation in $^{18}O/^{16}O$ of Modern Precipitation and River Water
732 across the Conterminous USA, *Hydrological Processes,* 19(20): 4121–46.
733 Elsner, M.M., Cuo, L., Voisin, N., Deems, J.S., Hamlet, A.F., Vano, J.A., Mickelson, K.E.B.,
734 Lee, S.Y., & Lettenmaier. D.P. (2010). Implications of 21st century climate change for
735 the hydrology of Washington State, *Climatic Change,* 102(2):225-260.
736 Fan, Y., Chen, Y., He, Q., Li, W., & Wang, Y. (2016). Isotopic Characterization of River Waters
737 and Water Source Identification in an Inland River, Central Asia, *Water,* 8(7): 286.
738 Fellman, J.B., Nagorski, S., Pyare, S., Vermilyea, W., Scott, D., & Hood, E. (2014). Stream
739 temperature response to variable glacier coverage in coastal watersheds of Southeast
740 Alaska, *Hydrological Processes*, 28: 2062 – 2073.

741 Fellman, J.B., Hood, E., Dryer, W., & Pyare, S. (2015). Stream physical characteristics impact
742 habitat quality for Pacifc salmon in two temperate coastal watersheds, *PLoS ONE*, 10(7):
743 e1032652.
744 Filipe, A.F., Quaglietta, L., Ferreira, M., Magalhães, M.F., & Beja, P. (2017). Geostatistical
745 Distribution Modelling of Two Invasive Crayfish across Dendritic Stream
746 Networks*, Biological Invasions,* 19(10): 2899–2912.
747 Friedman, I., & Smith, G.I. (1970). Deuterium Content of Snow Cores from Sierra Nevada Area,
748 *Science,* 169(3944): 467–70.
749 Gat, J.R. (1996). Oxygen and Hydrogen Isotopes in the Hydrologic Cycle, *Annual Review of*
750 *Earth and Planetary Sciences,* 24(1): 225–62.
751 Grasby, S.E., & Lepitzki, D.A.W. (2002). Physical and chemical properties of the Sulphur
752 Mountain thermal springs, Banff National Park, and implications for endangered snails,
753 *Canadian Journal of Earth Sciences*, 39: 1349–1361.
754 Guan, H., Simmons, C., & Love, A. (2009). Orographic controls on rain water isotope
755 distribution in the Mount Lofty Ranges, South Australia, *Journal of Hydrology*, 372: 255-
756 264.
757 Hill, R.A., Weber, M.H., Leibowitz, S.G., Olsen, A.R., & Thornbrugh, D.J. (2015). The Stream-
758 Catchment (StreamCat) Dataset: A database of watershed metrics for the conterminous
759 United States, *Journal of the American Water Resources Association*, 51(1): 120-128.
760 Hobson, K.A., & Wassenaar, L.I. (1997). Linking Breeding and Wintering Grounds of
761 Neotropical Migrant Songbirds Using Stable Hydrogen Isotopic Analysis of
762 Feathers, *Oecologia,* 109(1): 142–48.

763 Ingraham, N.L., & Taylor, B.E. (1991). Light Stable Isotope Systematics of Large-Scale
764 Hydrologic Regimes in California and Nevada, *Water Resources Research,* 27(1): 77–90.
765 Isaak, D.J., Peterson, E.E., Ver Hoef, J.M., Wenger, S.J., Falke, J.A., Torgersen, C.E., Sowder,
766 C., Steel, E.A., Fortin, M.J., Jornan, C.E., Ruesch, A.S., Som, N., Monestiez, P. (2014).
767 Applications of Spatial Statistical Network Models to Stream Data: Spatial Statistical
768 Network Models for Stream Data, *Wiley Interdisciplinary Reviews: Water,* 1(3): 277–94.
769 Jasechko, S., Kirchner, J.W., Welker, J.M., & McDonnell, J.J.. (2016). Substantial Proportion of
770 Global Streamflow Less than Three Months Old, *Nature Geoscience,* 9(2): 126–29.
771 Katsuyama, M., Yoshioka, T., & Konohira, E. (2015). Spatial Distribution of Oxygen-18 and
772 Deuterium in Stream Waters across the Japanese Archipelago, *Hydrology and Earth*
773 *System Sciences,* 19(3): 1577–88.
774 Kendall, C., & Coplen, T.B. (2001). Distribution of oxygen-18 and deuterium in river waters
775 across the United States, *Hydrological Processes,* 15: 1363–1393.
776 Koeniger, P., Leibundgut, C., & Stichler, W. (2009). Spatial and temporal characterisation of
777 stable isotopes in river water as indicators of groundwater contribution and confirmation
778 of modelling results; a study of the Weser river, Germany, *Isotopes in Environmental and*
779 *Health Studies,* 45: 289–302.
780 Lechler, A.R., & Niemi, N.A. (2011). Controls on the Spatial Variability of Modern Meteoric
781 18O: Empirical Constraints from the Western U.S. and East Asia and Implications for
782 Stable Isotope Studies, *American Journal of Science,* 311(8): 664–700.
783 Liu, F., Williams, M.W., & Caine, N. (2004). Source Waters and Flow Paths in an Alpine
784 Catchment, Colorado Front Range, United States, *Water Resources Research,* 40:
785 W09401.

786 Lucero, Y., Steel, E.A., Burnett, K.M., & Christiansen, K. (2011). Untangling Human
787 Development and Natural Gradients: Implications of Underlying Correlation Structure
788 for Linking Landscapes and Riverine Ecosystems, *River Systems,* 19(3): 207–24.
789 McGuire, K.J., McDonnell, J.J., Weiler, M., Kendall, C., McGlynn, B.L., Welker, J.M., &
790 Seibert, J. (2005). The Role of Topography on Catchment-Scale Water Residence Time,
791 *Water Resources Research,* 41: W05002.
792 McGuire, K.J., & McDonnell, J.J. (2006). A review and evaluation of catchment transit time
793 modeling. *Journal of Hydrology* 330: 543–563.
794 McGuire, K.J., Torgersen, C.E., Likens, G.E., Buso, D.C., Lowe, W.H., & Bailey, S.W. (2014).
795 Network Analysis Reveals Multiscale Controls on Streamwater Chemistry, *Proceedings*
796 *of the National Academy of Sciences,* 111(19): 7030–35.
797 McMahon, K.W., Hamady, L.L., & Thorrold, S.R. (2013). A Review of Ecogeochemistry
798 Approaches to Estimating Movements of Marine Animals, *Limnology and*
799 *Oceanography,* 58(2): 697–714.
800 Moran, T.A., Marshall, S.J., Evans, E.C., & Sinclair, K.E. (2007). Altitudinal Gradients of Stable
801 Isotopes in Lee-Slope Precipitation in the Canadian Rocky Mountains, *Arctic, Antarctic,*
802 *and Alpine Research,* 39(3): 455–67.
803 Mote, P.W., & Salathé, E.P. Jr. (2010). Future climate in the Pacific Northwest, *Climateic*
804 *Change,* 102(1-2): 29-50.
805 Mountain, N., James, A.L., & Chutko, K. (2015). Groundwater and Surface Water Influences on
806 Streamflow in a Mesoscale Precambrian Shield Catchment: Analysing Summer Sources
807 of Streamflow Using Stable Water Isoscapes, *Hydrological Processes,* 29(18*):* 3941–53.

808 Murray, K., & Conner, M.M. (2009). Methods to quantify variable importance: implications for
809 the analysis of noisy ecological data, *Ecology,* 90(2): 348-355.
810 Nickolas, L.B., Segura, C., & Brooks, J.R. (2017). The Influence of Lithology on Surface Water
811 Sources, *Hydrological Processes,* 31(10): 1913–25.
812 Neiman, P.J., Schick, L.J., Ralph, F.M., Hughes, M., & Wick, G.A. (2011). Flooding in western
813 Washington: The connection to atmospheric rivers, *Journal of Hydrometeorology,* 12(6):
814 1337–1358.
815 Peng, T.R., Chen, K.Y., Zhan, W.J., Lu, W.C., & Tong, L.T.J. (2015). Use of stable water
816 isotopes to identify hydrological processes of meteoric water in montane catchments,
817 *Hydrological Processes*, 29: 4957-4967.
818 Peterson, E.E., & Ver Hoef, J.M. (2010). A mixed-model moving-average approach to
819 geostatistical modeling in stream networks, *Ecology,* 91: 644-651
820 Peterson, E.E., & Ver Hoef, J.M. (2014). STARS: An ArcGIS toolset used to calculate the
821 spatial information needed to fit spatial statistical models to stream network data, *Journal*
822 *of Statistical Software*, 56(2): 1-17.
823 Poage, M.A., & Chamberlain, C.P. (2001). Empirical Relationships between Elevation and the
824 Stable Isotope Composition of Precipitation and Surface Waters: Considerations for
825 Studies of Paleoelevation Change, *American Journal of Science,* 301(1): 1–15.
826 Payn, R.A., Gooseff, M.N., McGlynn, B.L., Bencala, K.E., & Wondzell, S.M. (2012). Exploring
827 changes in the spatial distribution of stream baseflow generation during a seasonal
828 recession*, Water Resources Research,* 48: W04519.

Rautio, A., & Korkka-Niemi, K. (2015). Chemical and isotopic tracers indicating groundwater/surface-water interaction within a boreal lake catchment in Finland, *Hydrogeology Journal,* 23(4):687-705.

Riedel, J.L., & Larrabee, M.A. (2016). Impact of Recent Glacial Recession on Summer Streamflow in the Skagit River, *Northwest Science,* 90(1): 5–22.

Rock, L., & Mayer, B. (2007). Isotope Hydrology of the Oldman River Basin, Southern Alberta, Canada, Hydrological Processes, 21(24): 3301–15.

Rodgers, P., Soulsby, C., & Waldron, S. (2005). Stable Isotope Tracers as Diagnostic Tools in Upscaling Flow Path Understanding and Residence Time Estimates in a Mountainous Mesoscale Catchment, *Hydrological Processes,* 19(11): 2291–2307.

Scheihing, K.W., Moya, C.E., Struck, U., Lictevout, E., & Tröger, U. (2018). Reassessing hydrological processes that control stable isotope tracers in groundwater of the Atacama Desert (Northern Chile), *Hydrology*, 5(1): 3.

Siler, N., Roe, G., & Durran, D. (2013). On the Dynamical Causes of Variability in the Rain-Shadow Effect: A Case Study of the Washington Cascades, *Journal of Hydrometeorology,* 14:122–139.

Singh, N.K., Emanuel, R.E., & McGlynn, B.L. (2016). Variability in Isotopic Composition of Base Flow in Two Headwater Streams of the Southern Appalachians, *Water Resources Research,* 52(6): 4264–79.

Steel, A.E., Sowder, C., & Peterson, E.E. (2016). Spatial and Temporal Variation of Water Temperature Regimes on the Snoqualmie River Network, *Journal of the American Water Resources Association,* 52(3): 769–87.

Steel, A.E., Marsha, A., Fullerton, A.H., Olden, J.D., Larkin, N.K., Lee, S.Y., & Ferguson, A. (2018). Thermal landscapes in a changing climate: biological implications of water temperature patterns in an extreme year, *Canadian Journal of Fisheries and Aquatic Sciences*, https://doi.org/10.1139/cjfas-2018-0244.

Tauge, C., & Grant, G.E. (2009). Groundwater dynamics mediate low-flow response to global warming in snow-dominated alpine regions, *Water Resources Research*, 45: W07421.

Trinh, D.A., Luu, M.T.N., & Le, Q.T.P. (2017). Use of stable isotopes to understand run-off generation processes in the Red River Delta, *Hydrological Processes,* 31: 3827–3843.

Vachon, R.W., Welker, J.M., White, J.W.C., & Vaughn, B.H. (2010). Monthly Precipitation Isoscapes ($\delta^{18}O$) of the United States: Connections with Surface Temperatures, Moisture Source Conditions, and Air Mass Trajectories, *Journal of Geophysical Research,* 115: D21126.

Ver Hoef, J.M., Peterson, E.E., & Theobald, D. (2006). Spatial statistical models that use flow and stream distance, *Environmental and Ecological Statistics,* 12:449-464.

Ver Hoef, J.M., & Peterson, E.E. (2010). A moving average approach to spatial statistical models of stream networks*, The Journal of the American Statistical Association,* 489: 6-18.

Ver Hoef, J.M., Peterson, E.E., Clifford, D., & Shah, R. (2014). SSN: An R package for spatial statistical modeling on stream networks, *The Journal of Statistical Software*, 56(3): 1-45.

Vespasiano, G., Apollaro, C., De Rosa, R., Muto, F., Larosa, S., Fiebig, J., Mulch, A., & Marini, L. (2015). The Small Spring Method (SSM) for the definition of stable isotope-elevation relationships in Northern Calabria (Southern Italy), *Applied Geochemistry*, 63: 333-346.

Walsh, C.& MacNally, R. (2013). hier.part: Hierarchical Partitioning. R package version 1.0-4. https://CRAN.R-project.org/package=hier.part.

874 Wang, N.L., Zhang, S.B., He, J.Q., Pu, J.C., Wu, X.B., & Jiang, X. (2009). Tracing the Major
875 Source Area of the Mountainous Runoff Generation of the Heihe River in Northwest
876 China Using Stable Isotope Technique, *Science Bulletin,* 54(16): 2751–57.
877 Wassenaar, L.I., Van Wilgenburg, S.L., Larson, K., & Hobson, K.A. (2009). A Groundwater
878 Isoscape (ΔD, Δ18O) for Mexico, *Journal of Geochemical Exploration,* 102(3): 123–36.
879 Wassenaar, L.I., Athanasopoulos, P., & Hendry, M.J. (2011). Isotope hydrology of precipitation,
880 surface and ground waters in the Okanagan Valley, British Columbia, Canada, *Journal of*
881 *Hydrology,* 411: 37-48.
882 West, J.B., Bowen, G.J., Dawson, T.E., & Tu, K.P., eds. (2010). Isoscapes: Understanding
883 Movement, Pattern, and Process on Earth through Isotope Mapping. Dordrecht; New
884 York: Springer.
885 Wolock, D.M., Winter, T.C., & McMahon, G. (2004). Delineation and evaluation of hydrologic-
886 landscape regions in the United States using geographic information system tools and
887 multivariate statistical analyses, *Environmental Management,* 34: 71-88.
888 Yeh, H.S., Lin, H.I., Lee, C.H., Hsu, K.C., & Wu, C.S. (2014). Identifying Seasonal
889 Groundwater Recharge Using Environmental Stable Isotopes, *Water,* 6(10): 2849–61.
890 Yonge, C.J., Goldenberg, L., & Krouse HR. (1989). An Isotope Study of Water Bodies along a
891 Traverse of Southwestern Canada. *Journal of Hydrology,* 106(3–4): 245–55.
892 Zimmerman, D.L., & Ver Hoef, J.M. (2017). The Torgegram for Fluvial Variography:
893 Characterizing Spatial Dependence on Stream Networks, *Journal of Computational and*
894 *Graphical Statistics,* 26(2): 253–64.
895
896

Figure 1: Geographic locations of study basins, the Snoqualmie (A), Green (B), Skagit (C), and Wenatchee (D) Rivers in Washington and Cowee Creek (E) in southeastern Alaska. Between 31-58 water samples were collected within each basin ($n_{Snoqualime} = 58$, $n_{Green} = 31$, $n_{Skagit} = 38$, $n_{Wenatchee} = 44$, $n_{Cowee} = 38$) and are shown in yellow. Red points indicate a major dam and blue shading indicates an ice mass.

Figure 2. Regressions of $\delta^{18}O$ values with MWE for samples collected during summer low flow for each basin. Lines represent the least squares relationships. Triangle points are mainstem sites and circle points are tributary sites. Points are colored according to the mean annual precipitation (MAP) within the upstream watershed.

Figure 3. Correlation matrices for the Snoqualmie, Green, Skagit, and Wenatchee Rivers, and Cowee Creek. Both isotope metrics and landscape covariates are included. Red indicates a negative correlation between two variables, and blue indicates a positive correlation. The darker the color, the stronger the correlation. See Table 2 for a description of covariates.

Figure 4. Semivariograms for raw $\delta^{18}O$ values, residual $\delta^{18}O$ values from the best-fit linear models, and residual $\delta^{18}O$ values from the best-fit SSNMs for the Snoqualmie and Wenatchee basins. Circles are proportional to the number of sites used to estimate each bin value.

Figure 5. Isoscapes from the Snoqualmie best-fit linear model (A), Snoqualmie best-fit SSNM (B), Wenatchee best-fit linear model (C), and Wenatchee best-fit SSNM (D). Colors represent predicted $\delta^{18}O$ values and the size of each point is inversely proportional to the prediction standard error.

Figure 6. Variance decomposition into the proportion of variation explained by covariates (blue), tail-up covariance structure (yellow), Euclidean covariance structure (red), and the nugget (gray) for each of the SSNMs (categories on the x-axis) in the Snoqualmie and Wenatchee basins. TU=tail-up; Euc=Euclidean; TU.Euc=tail-up and Euclidean.

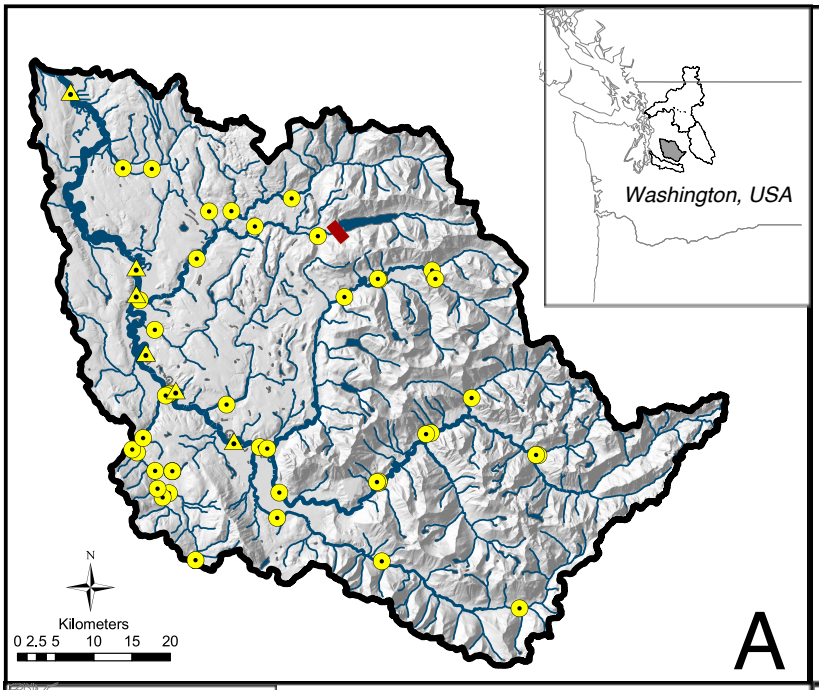
Washington, USA
N
Kilometers
0 2,5 5 10 15 20
A

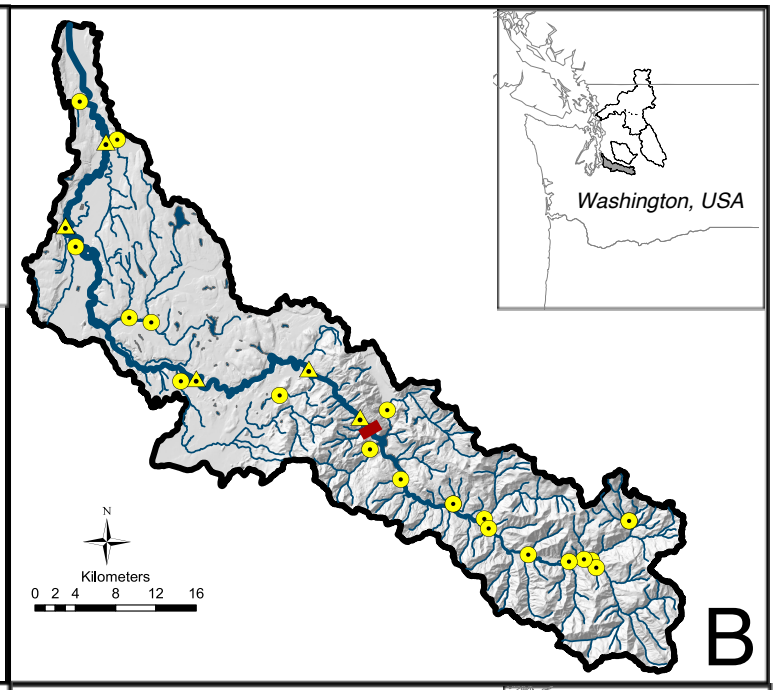
Washington, USA
N
Kilometers
0 2 4 8 12 16
B

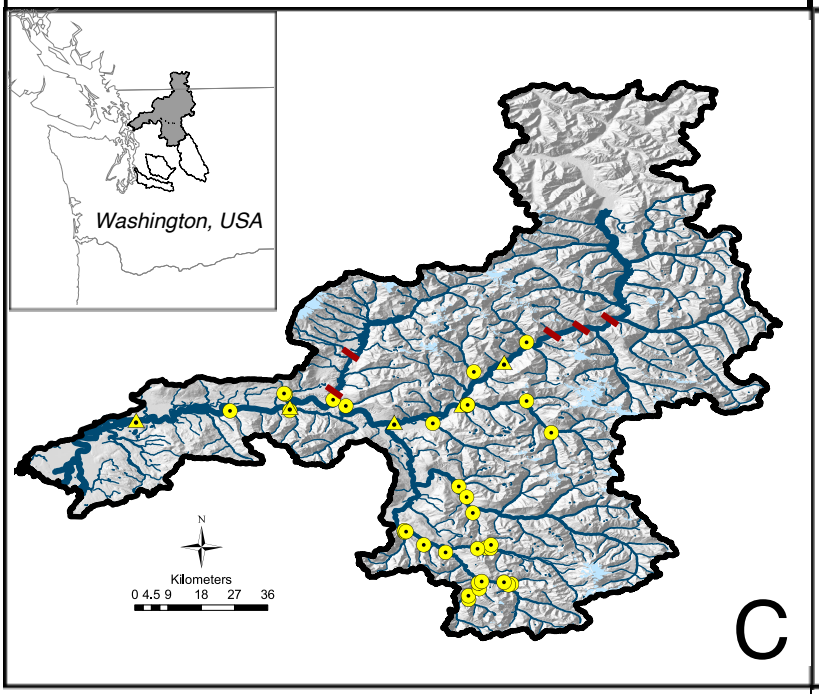
Washington, USA
N
Kilometers
0 4,5 9 18 27 36
C

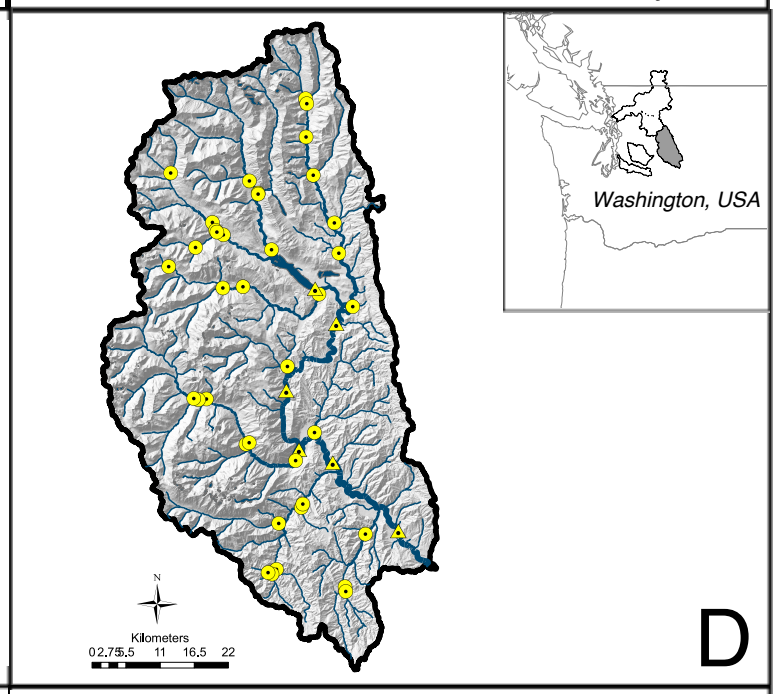
Washington, USA
N
Kilometers
0 2,75 5,5 11 16,5 22
D

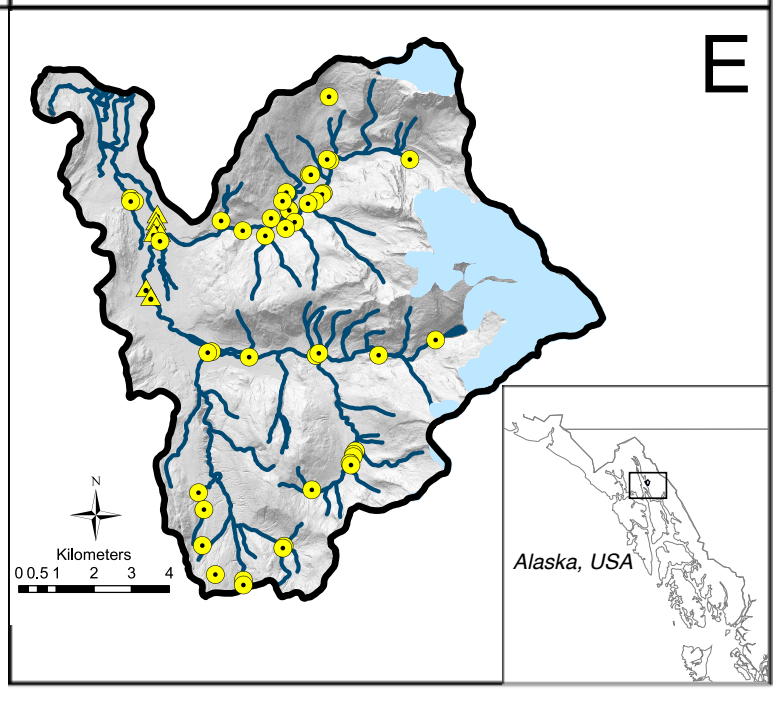
E
N
Kilometers
0 0,5 1 2 3 4
Alaska, USA

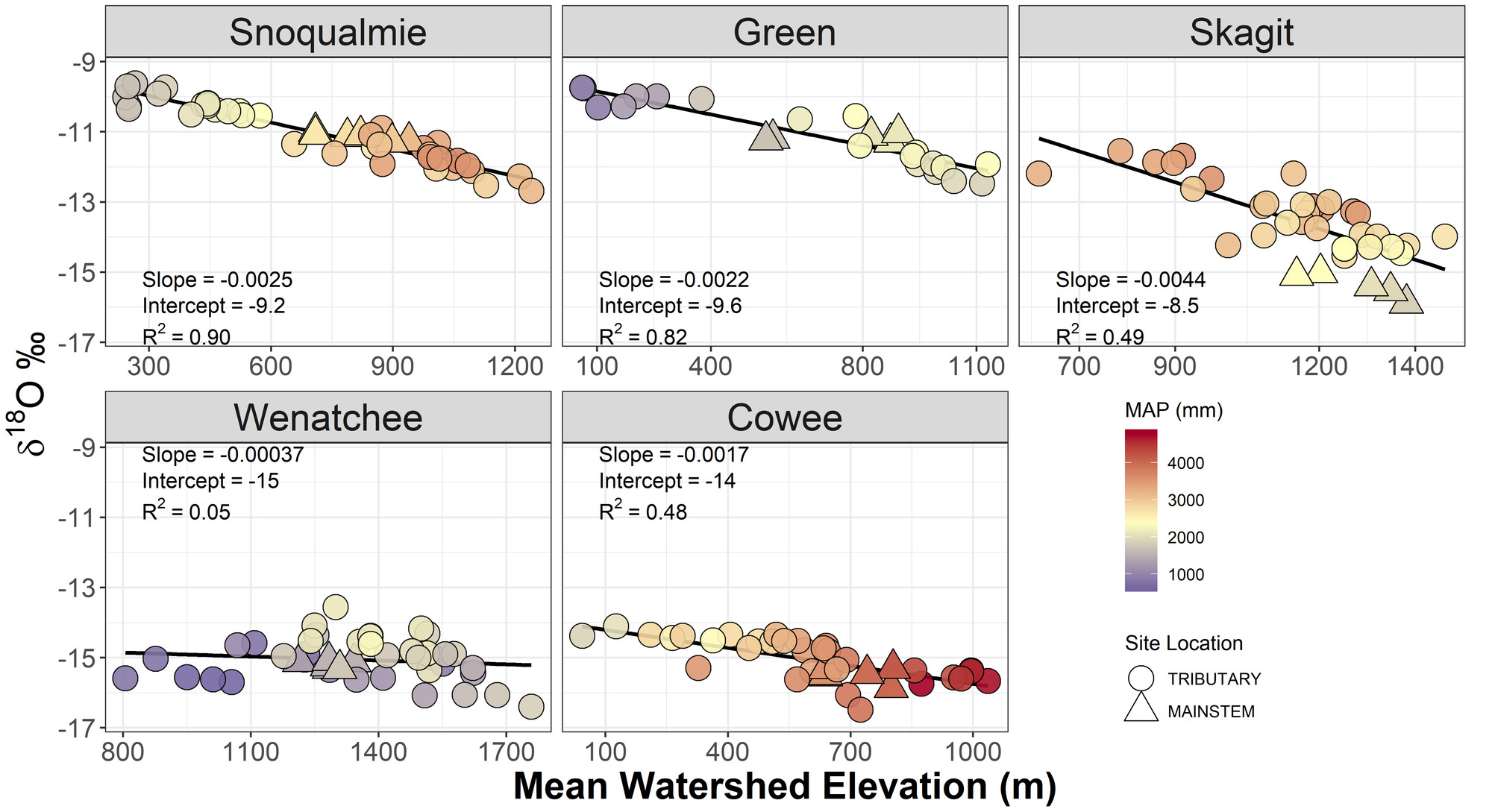
Snoqualmie
Slope = -0.0025
Intercept = -9.2
R2 = 0.90
Green
Slope = -0.0022
Intercept = -9.6
R2 = 0.82
Skagit
Slope = -0.0044
Intercept = -8.5
R2 = 0.49
Wenatchee
Slope = -0.00037
Intercept = -15
R2 = 0.05
Cowee
Slope = -0.0017
Intercept = -14
R2 = 0.48
δ18O ‰
Mean Watershed Elevation (m)
MAP (mm)
4000
3000
2000
1000
Site Location
TRIBUTARY
MAINSTEM

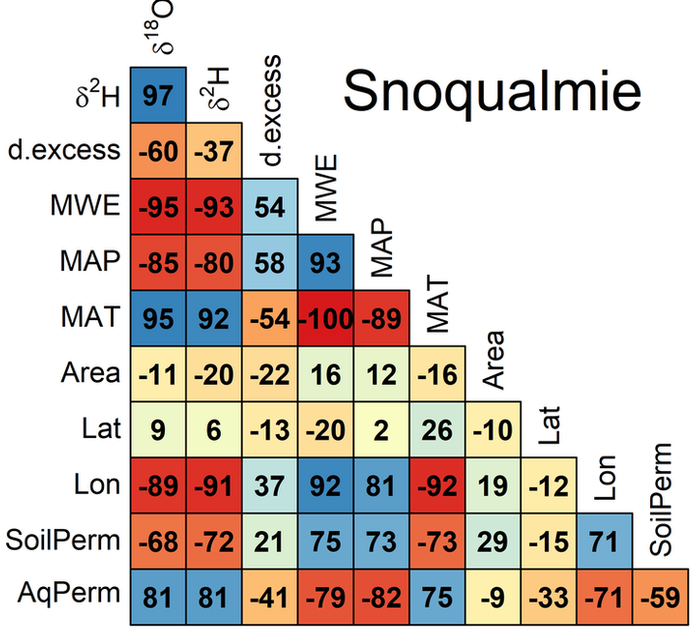
Snoqualmie
δ18O
δ2H
d.excess
MWE
MAP
MAT
Area
Lat
Lon
SoilPerm
δ2H 97
d.excess -60 -37
MWE -95 -93 54
MAP -85 -80 58 93
MAT 95 92 -54 -100 -89
Area -11 -20 -22 16 12 -16
Lat 9 6 -13 -20 2 26 -10
Lon -89 -91 37 92 81 -92 19 -12
SoilPerm -68 -72 21 75 73 -73 29 -15 71
AqPerm 81 81 -41 -79 -82 75 -9 -33 -71 -59

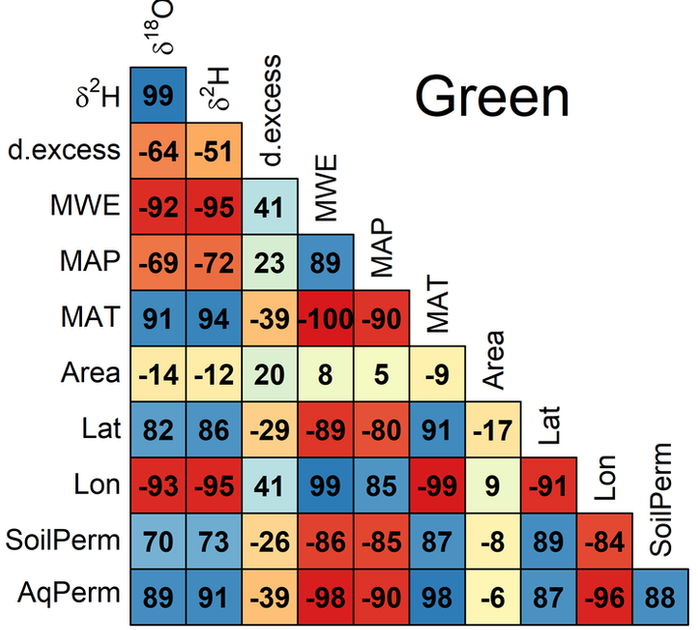
Green
δ18O
δ2H
d.excess
MWE
MAP
MAT
Area
Lat
Lon
SoilPerm
δ2H 99
d.excess -64 -51
MWE -92 -95 41
MAP -69 -72 23 89
MAT 91 94 -39 -100 -90
Area -14 -12 20 8 5 -9
Lat 82 86 -29 -89 -80 91 -17
Lon -93 -95 41 99 85 -99 9 -91
SoilPerm 70 73 -26 -86 -85 87 -8 89 -84
AqPerm 89 91 -39 -98 -90 98 -6 87 -96 88

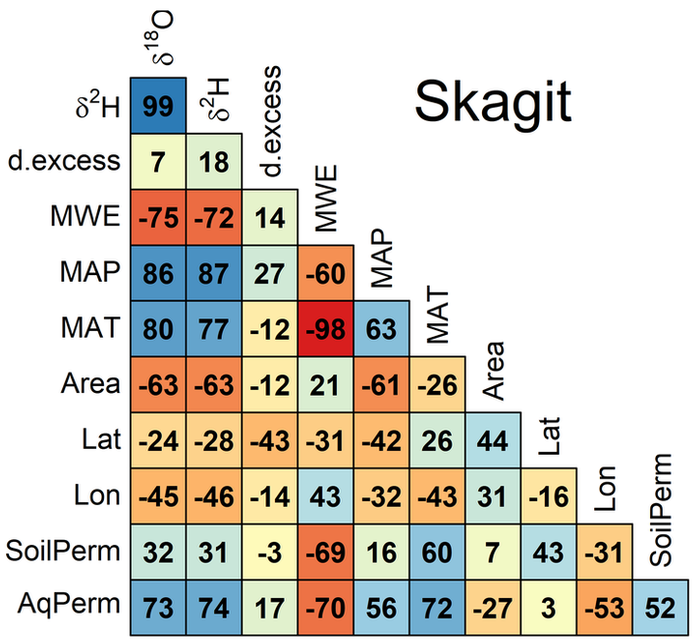
Skagit
δ18O
δ2H
d.excess
MWE
MAP
MAT
Area
Lat
Lon
SoilPerm
δ2H 99
d.excess 7 18
MWE -75 -72 14
MAP 86 87 27 -60
MAT 80 77 -12 -98 63
Area -63 -63 -12 21 -61 -26
Lat -24 -28 -43 -31 -42 26 44
Lon -45 -46 -14 43 -32 -43 31 -16
SoilPerm 32 31 -3 -69 16 60 7 43 -31
AqPerm 73 74 17 -70 56 72 -27 3 -53 52

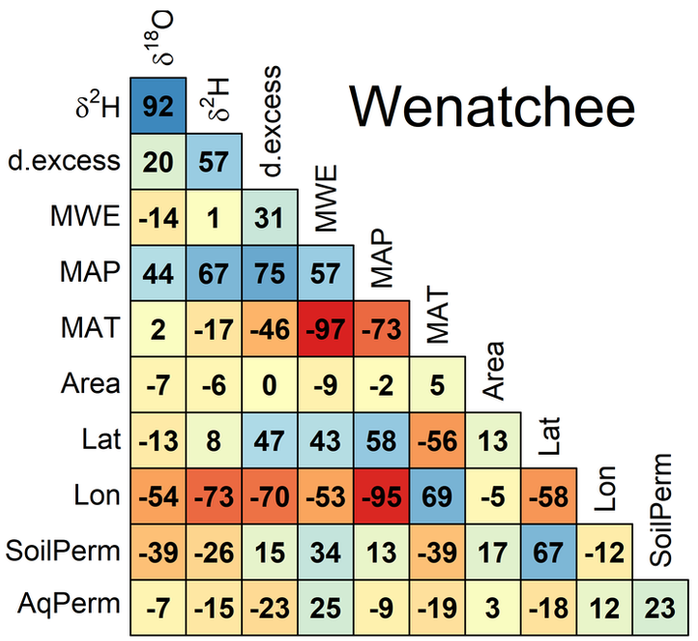
Wenatchee
δ18O
δ2H
d.excess
MWE
MAP
MAT
Area
Lat
Lon
SoilPerm
δ2H 92
d.excess 20 57
MWE -14 1 31
MAP 44 67 75 57
MAT 2 -17 -46 -97 -73
Area -7 -6 0 -9 -2 5
Lat -13 8 47 43 58 -56 13
Lon -54 -73 -70 -53 -95 69 -5 -58
SoilPerm -39 -26 15 34 13 -39 17 67 -12
AqPerm -7 -15 -23 25 -9 -19 3 -18 12 23

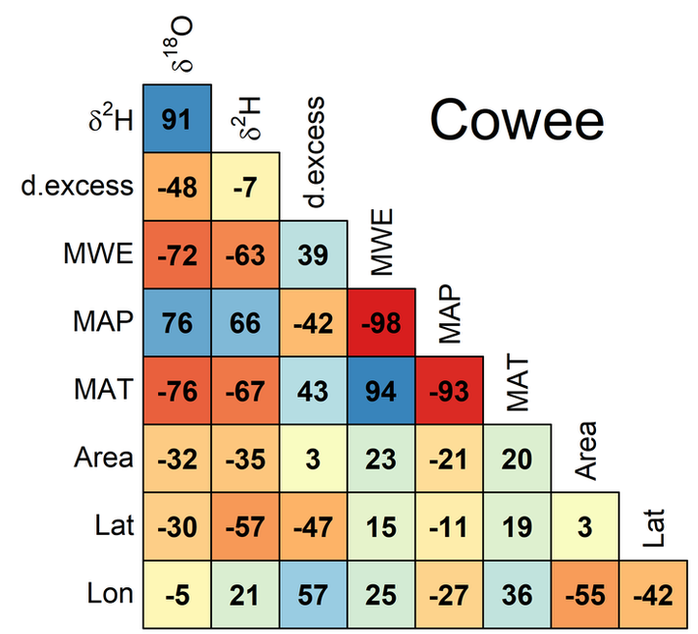
Cowee
δ18O
δ2H
d.excess
MWE
MAP
MAT
Area
Lat
Lon
δ2H 91
d.excess -48 -7
MWE -72 -63 39
MAP 76 66 -42 -98
MAT -76 -67 43 94 -93
Area -32 -35 3 23 -21 20
Lat -30 -57 -47 15 -11 19 3
Lon -5 21 57 25 -27 36 -55 -42

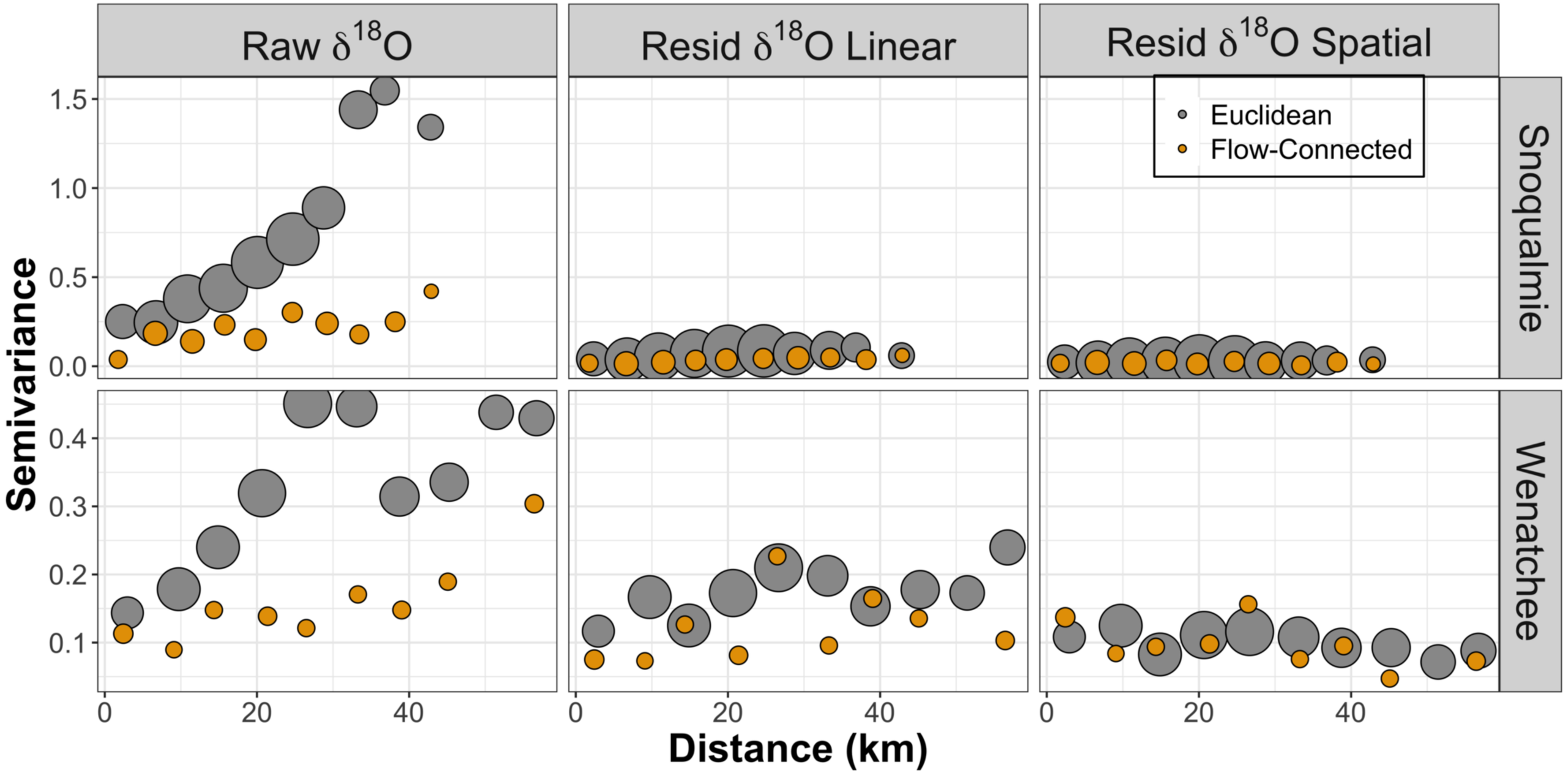
Raw δ18O
Resid δ18O Linear
Resid δ18O Spatial
Euclidean
Flow-Connected
Snoqualmie
Wenatchee
Semivariance
Distance (km)
0.0
0.5
1.0
1.5
0.1
0.2
0.3
0.4
0
20
40

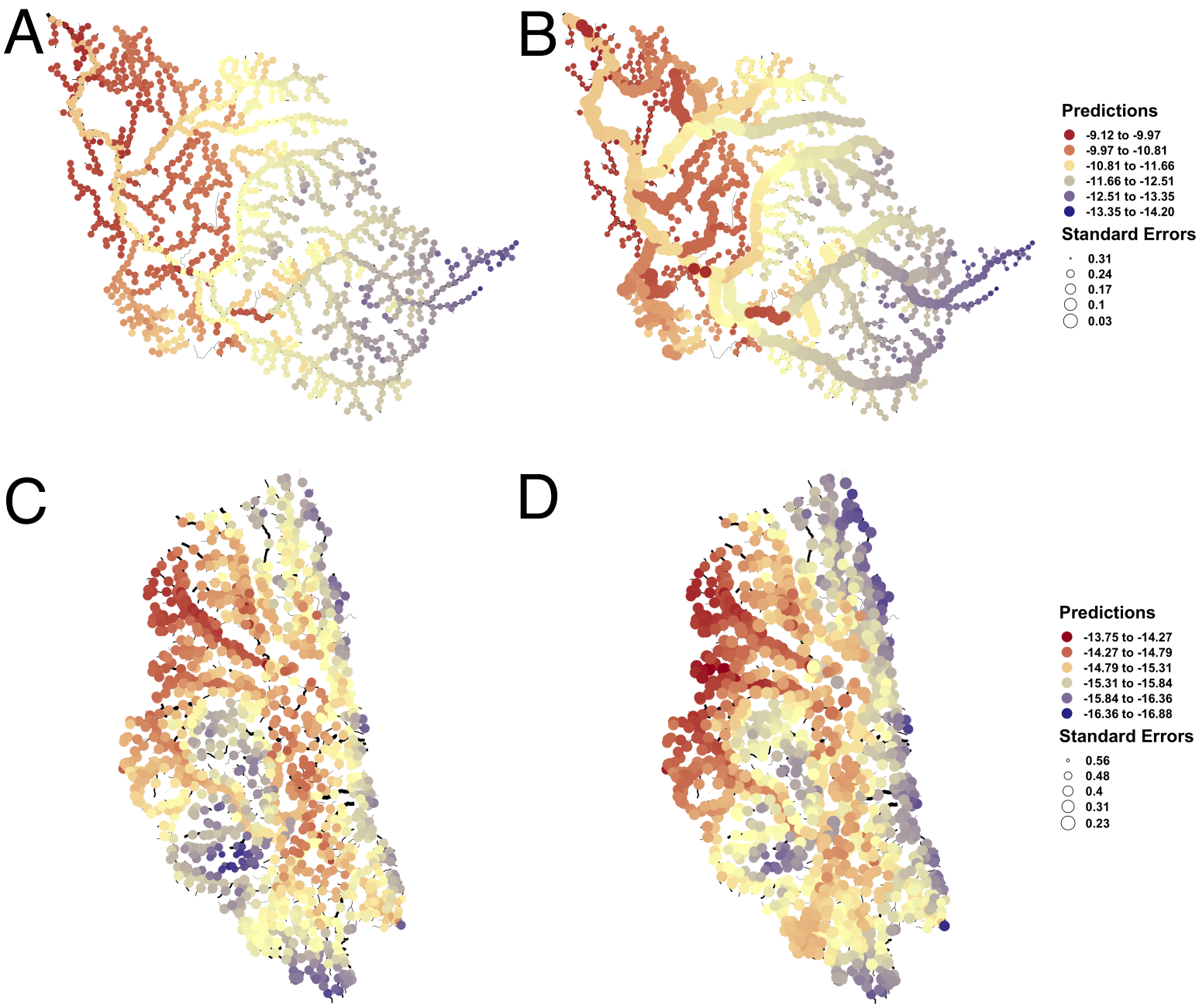
A
B
Predictions
-9.12 to -9.97
-9.97 to -10.81
-10.81 to -11.66
-11.66 to -12.51
-12.51 to -13.35
-13.35 to -14.20
Standard Errors
0.31
0.24
0.17
0.1
0.03
C
D
Predictions
-13.75 to -14.27
-14.27 to -14.79
-14.79 to -15.31
-15.31 to -15.84
-15.84 to -16.36
-16.36 to -16.88
Standard Errors
0.56
0.48
0.4
0.31
0.23

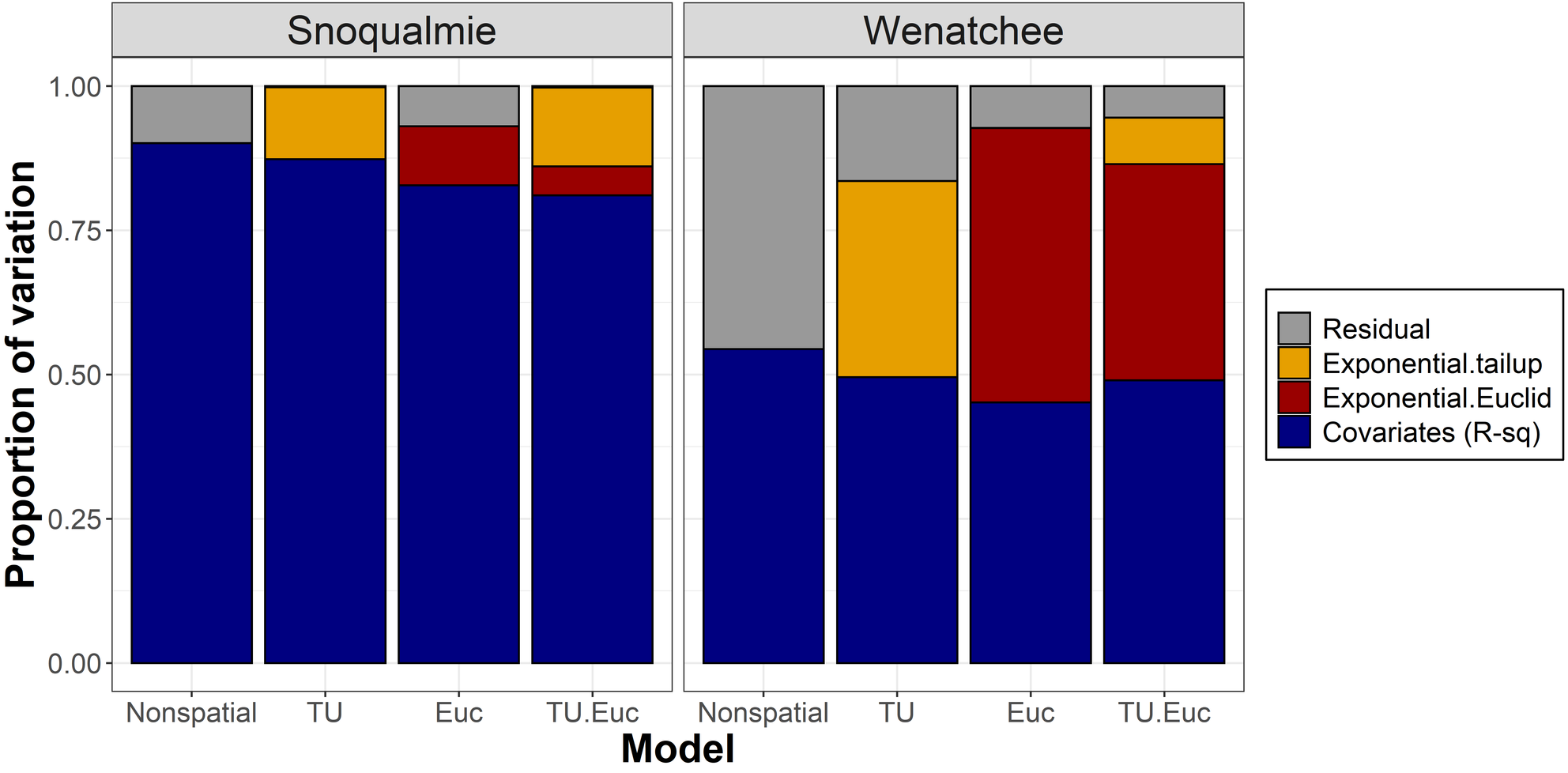
Snoqualmie
Wenatchee
1.00
0.75
0.50
0.25
0.00
Proportion of variation
Nonspatial
TU
Euc
TU.Euc
Model
Residual
Exponential.tailup
Exponential.Euclid
Covariates (R-sq)

Table 1: Climate and physical characteristics for each basin**.**

		Snoqualmie	Green	Skagit	Wenatchee	Cowee
Mean Annual Temperature (C°)	Mean	8.16	8.25	6.36	6.15	1.76
	Maximum	11.55	11.84	10.68	11.13	5.09
	Minimum	1.77	4.04	-0.22	-0.12	-0.38
Mean Annual Precipitation (mm)	Mean	2,435	1,810	2,154	1,210	3,568
	Maximum	4,304	2,727	4,948	2,940	4,792
	Minimum	1,102	925	711	232	1,792
Elevation (m)	Mean	629	580	946	1,087	638
	Maximum	1,876	1,500	3,283	2,390	1,791
	Minimum	8	5	1	194	1
Basin Size (km^2)		1,793	1,185	8,163	3,440	118

Table 2: List of covariates considered for inclusion in each model. Here, "watershed" indicates the upstream area draining to a sample.

Covariate	Abbreviation	Description	Unit	Data Source
Elevation	MWE	Mean watershed elevation	m	NED DEM model
Mean Annual Precipitation	MAP	Mean watershed 30-year average (1981-2010) annual normal precipitation	mm	PRISM Climate Group, EPA StreamCat (Hill et al. 2015)
Mean Average Air Temperature	MAT	Mean watershed 30-year average (1981-2010) annual mean air temperature	C°	PRISM Climate Group, EPA StreamCat (Hill et al. 2015)
Area	Area	Log transformed watershed area	$\log(km^2)$	NED DEM model
Latitude	Lat	Latitude of watershed centroid	degree	
Longitude	Lon	Longitude of watershed centroid	degree	
Soil Permeability	SoilPerm	Mean watershed soil permeability	cm/hour	STATSGO, StreamCat (Hill et al. 2015)
Bedrock Permeability	AqPerm	Mean watershed bedrock permeability	dimensionless; 1-7 based on lithology	USGS Hydrologic Landscape Regions (Wolock et al. 2004)

Table 3. Best fit linear models from the Snoqualmie, Green, Skagit, Wenatchee, and Cowee basins. The independent effect weight is the percentage of explained variance by each covariate.

Basin	Covariates	Covariate Coefficient (SE)	Independent Effect Weight (%)	R^2	RMSPE
Snoqualmie	MWE	-0.0025 (0.00013)	100	0.90	0.26
Green	MWE	-0.0022 (0.00020)	100	0.82	0.35
Skagit	MWE	-0.0018 (0.00051)	21	0.87	0.38
	MAP	0.00095 (0.00021)	33		
	Area	-0.00015 (0.000041)	26		
	Aquifer Permeability	0.40 (0.14)	20		
Wenatchee	Longitude	-2.99 (0.44)	70	0.47	0.42
	MWE	-0.0016 (0.00034)	30		
Cowee	MWE	-0.0017 (0.00028)	100	0.48	0.41

Table 4. Model fit statistics from SSNMs in the Snoqualmie and Wenatchee basins. Variance component values are the percentage of variance explained by fixed effects (covariates) and spatial error. Models in bold were selected as the best fit models.

	Model	Covariate	Covariate Coefficient (SE)	RMSPE	AIC	R^2	Variance Component	
							Fixed effects (%)	Spatial error (%)
Snoqualmie	Nugget	MWE	-0.0025 (0.00013)	0.26	25.80	0.90	90	-
	Tail-up	**MWE**	**-0.0026 (0.00015)**	**0.16**	**-5.97**	**0.96**	**87**	**9**
	Euclid	MWE	-0.0025 (0.00017)	0.23	19.35	0.89	83	6
	Euclid + Tail-up	MWE	-0.0026 (0.00019)	0.17	-4.18	0.96	81	15
Wenatchee	Nugget	Longitude	-2.99 (0.44)	0.42	61.07	0.47	47	-
		MWE	-0.0016 (0.00034)					
	Tail-up	Longitude	-3.24 (0.52)	0.37	53.29	0.61	45	16
		MWE	-0.0016 (0.00037)					
	Euclid	Longitude	-3.22 (0.58)	0.33	51.24	0.67	42	24
		MWE	-0.0013 (0.00033)					
	Euclid + Tail-up	**Longitude**	**-3.73 (0.62)**	**0.31**	**51.67**	**0.71**	**45**	**26**
		MWE	**-0.0015 (0.00034)**					